universität wien

MASTERARBEIT / MASTER'S THESIS

Titel der Masterarbeit / Title of the Master's Thesis

„Multiplicity Among Young Stellar Objects in Orion A“

verfasst von / submitted by

Christine Ackerl, BSc

angestrebter akademischer Grad / in partial fulfilment of the requirements for the degree of

Master of Science (MSc)

Wien, 2020 / Vienna, 2020

Studienkennzahl lt. Studienblatt / degree programme code as it appears on the student record sheet:	A 066 861
Studienrichtung lt. Studienblatt / degree programme as it appears on the student record sheet:	Astronomie
Betreut von / Supervisor:	Univ.-Prof. Dr. João Alves,
Mitbetreut von / Co-Supervisor:	Dr. Stefan Meingast, Bakk. MSc

Für Leon und Mama,
danke, dass ihr immer an mich glaubt.

How was your day at university? Did you discover something new and exciting?

— Leon Ackerl

Abstract

In order to shed light on the dependencies of stellar multiplicity on evolutionary state and environmental properties, I analyzed the multiplicity properties of the largest sample of young visual binaries in one single star-forming cloud, the rich and nearby Orion A. Due to the large input dataset of 3386 YSOs, the analysis required the development of an Automated COmpanion DEtection routine (ACODER). The YSO catalog was assembled from the catalogs from Großschedl et al. (2018b) and Pillitteri et al. (2013), who analyze YSOs from all evolutionary states, from Class 0 to Class III. The image data was taken from the Vienna Survey in Orion (VISION, Meingast et al., 2016), and maps the entire Orion A cloud. The survey provides seeing limited ESO-VISTA images and JHKs-photometry for 800,000 sources. It covers a vast range of different star-forming environments, from well known dense clusters to isolated and quiescent (Taurus-like) environments. The binary sample is sensitive to separations $>$ 0.8 arcsec, which corresponds to 330 AU at a distance of 414 pc. Out of the 3386 initial target YSOs, 1835 passed the selection criteria and were successfully processed with ACODER. These 1835 primary YSOs in total, have 318 companion candidates CCs, within a separation range of 5 arcsec. 242 of these CCs are estimated to be line of sight contaminants, leaving 76 bona fide companions. The estimated companion fraction for the total sample is 4.16 $\pm$ 0.10 %. The sample of YSOs is further divided into different classes of YSOs, different regions of Orion A, as well as different YSO surface densities. I find strong evidence for a decrease of companion fractions towards more evolved YSOs in all samples. The decrease is most prominent in the eastern and the low-density sample. The total CF of the western sample (2.03 $\pm$ 0.7 %) is found to be lower than the CF of the eastern sample (7.25 $\pm$ 0.28 %) These findings seem to suggest that multiple systems decay with age, even in quiescent environments and that this decay is accelerated in higher density environments. However, I find evidence for a higher total CF of 6.38 $\pm$ 0.23 % in the high-density sample, when compared to the CF of the low-density sample of 2.58 $\pm$ 0.09 %. This increase of the CF towards higher densities is in tension with the conclusion above and gives reason for discussion.

Zusammenfassung

Um die Abhängigkeit von stellarer Multiplizität von der Entwicklungsstufe der Sterne und den Eigenschaften ihrer Umgebung zu beleuchten, wird in dieser Arbeit die Multiplizität der größten Stichprobe von jungen, optischen Doppelsternen, in einer einzigen sternerzeugenden Wolke, Orion A analysiert. Aufgrund des großen Datensatzes von 3386 jungen stellaren Objekten (YSOs) war für das Auffinden von Begleitsternen die Entwicklung einer automatisierten Routine (ACODER) notwendig. Der Katalog von Zielobjekten setzt sich aus den Katalogen von Großschedl et al. (2018b) und Pillitteri et al. (2013) zusammen und beinhaltet junge stellare Objekte (YSOs) in allen Entwicklungsstufen, von Class 0 bis Class III Objekten. Das Bildmaterial für diese Arbeit stammt vom Vienna Survey in Orion (VISION, Meingast et al., 2016), welcher die gesamte Sternentstehungsregion Orion A abbildet. Die seeing-begrenzten Beobachtungen wurden mit dem ESO-VISTA Teleskop durchgeführt und beinhalten J, H und Ks Photometrie für 800.000 Quellen. Die Beobachtung deckt eine Vielzahl von verschiedenen Sternenstehungsumgebungen ab, von bekannten dichten Sternhaufen, bis hin zu ruhigen, isolierten (Taurus-artigen) Regionen. Diese Studie ist in der Lage, Doppensterne mit Abständen von 0.8 Bogensekunden (das entspricht $\sim$ 330 Astronomischen Einheiten (AU) bei einer Entfernung von 414 pc) zu detektieren. Von den 3386 anfänglichen YSOs erfüllen 1835 die Auswahlkriterien und konnten erfolgreich mit ACODER analysiert werden. Diese 1835 Primärquellen haben insgesamt 318 potenzielle Begleitsterne (companion candidates,CCs), innerhalb eines Abstandes von 5 Bogensekunden. Die Berechnung der durchschnittlichen Anzahl von Hintergrundquellen pro projizierter Fläche ergibt, dass 242 von diesen CC Detektionen der Verunreinigungen durch Hintergrundquellen zuzuschreiben sind. Folglich sind 76 der CCs tatsächliche Begleitsterne. Die errechnete Begleitsternhäufigkeit (companion fraction, CF) für das gesamte Sample ist 4.16 $\pm$ 0.10 %. Das Sample wurde weiter aufgeteilt, in Gruppen von unterschiedliche YSO Klassen, verschiedenen Regionen von Orion A und verschiedenen YSO-Oberflächendichten. Die Resultate zeigen, dass die CF mit zunehmendem Entwicklungsgrad der YSOs in allen Samples abnehmen. Am stärksten ausgeprägt ist dieser Trend im östlichen Sample und in jenem mit geringer

Sterndichte. Für das westliche Sample wird eine CF von 2.03 $\pm$ 0.7 % berechnet, welche mehr als drei mal geringer ist als die von 7.25 $\pm$ 0.28 % für das östliche Sample. Diese Resultate scheinen darauf hinzudeuten, dass Mehrfachsternsysteme mit zunehmendem Alter zerfallen, auch dann, wenn sie sich in einer relativ ruhigen Umgebung befinden. Dieser Zerfall wird in Regionen mit höherer Dichte scheinbar beschleunigt. Dem steht entgegen, dass für das Sample die CF von 6.38 $\pm$ 0.23 %, die für das Sample mit höherer Oberflächendichte, wesentlich höher ist als die CF von 2.58 $\pm$ 0.09 %, die für das Sample mit geringerer Oberflächendichte. Dieser Anstieg der CF mit der Dichte der Umgebung, scheint den vorherig erwähnten Ergebnissen zu widersprechen und gibt Anlass zur Diskussion.

Contents

Chapter 1

Introduction

1.1 Understanding star formation

While the basic principles of the physics involved in star formation have been understood for roughly one century (e.g. Spitzer, 1941; Whipple, 1946; Bok and Reilly, 1947), we are still seeking answers to some of the most fundamental questions on this important process. It seems, that the more we know about star formation, the more complex it becomes. Molecular clouds for example are never spherical, stellar birth places are filamentary and they don't simply collapse to form a single star which consumes all the gas, but fragment into multiple cloud cores, some of which do not form any stars, while some fragment again to form multiple stars. The majority of the gas and dust is left to form complex nebulae, which in turn, are affected by the recently formed stars or the violent death of the most massive stars. Gaining a complete understanding of the processes involved in forming new stars is complicated even more by the vast range of length scales involved in the path from a giant molecular cloud to a protostar. In addition, some of the most fundamental processes happen on astronomically short timescales and therefore appear to us as rather rare events. The interests of researchers in the field of star formation are as vastly distributed as these processes, ranging from large scale molecular line observations towards giant molecular clouds, to simulations of protoplanetary disk. The goal of all these research efforts remains the same, namely to find one set of universal laws that describes how exactly interstellar gas and dust is transformed into stars. This fundamental endeavor has been challenged with findings of very different properties of young stars in different star forming regions, one of these properties is stellar multiplicity. These findings suggest, that the physics we aim to fully understand, does not describe one single star formation scenario, which is responsible

for all the observed phenomena, but rather many, which are determined by the initial conditions. The goal to fully understand star formation therefore has become a quest for the hopefully universal links between different properties of stellar birth sites and the stellar output they "produce". In other words, we need to understand the dependencies of Young Stellar Object (YSO) properties, on the physical parameters of their formation environment, such as metallicity, density, or age of the universe.

The study of such YSOs however is not as straight forward as the study of their evolved siblings that form the galactic field population. On the galactic scale, star formation is not a rare event. Even with its comparably low star formation rate (SFR), on average, our galaxy forms $\sim$ 1.65 solar masses ($M_\odot$) of new stars per year (Licquia and Newman, 2015). This means, that our galaxy should host $\sim$ 5 Million $M_\odot$ in stars that are younger than 3 Million years. However, compared to the stellar mass of our galaxy's disk of $\sim$ $5.17{\cdot}10^{10}$ $M_\odot$ (Licquia and Newman, 2015), this number is extremely low. It means that only $\sim$ 0.01 % of the stars in the Milky Way's disk are younger than 3 Million years.
While this is a very rough calculation, which doesn't take into account the different lifetimes of stars, it serves the purpose of illustrating the relations and demonstrates a general problem of star formation research, which is, that the number of YSOs in the solar vicinity is extremely low, when compared to the number of evolved field stars. For massive stars, it is much lower even, since they are the rarest to be formed and the fastest to terminate their lives. Studying YSOs and especially sampling large numbers of different types of YSOs is therefore much harder, than studying Main Sequence (MS) stars, just because of simple number counts. Despite this fact, luckily there are a number of well studied star forming regions close to the sun, e.g. Perseus, Taurus, Ophiuchus, and the richest of them all, Orion A.

On top of that, by their nature, the earliest stages of stellar evolution hide in dust clouds, which block the visible light and make observations even harder. Where stars form, dust is ubiquitous and UV and optical radiation get absorbed by dust grains and molecules. Towards longer wavelengths however, the dust becomes more and more transparent. A famous example for the wavelength dependency of dust extinction are the images of the molecular cloud Barnard 68 by Alves et al. (2001). Figure 1.1 shows how the extinction of the clouds background stars decreases towards longer wavelengths.

Studying longer wavelength emission, i.e. infrared (IR) or radio radiation is therefore essential in order to understand star formation. Although radio astronomy with large telescope arrays enable us to resolve young stars in unprecedented detail (Figure 1.2

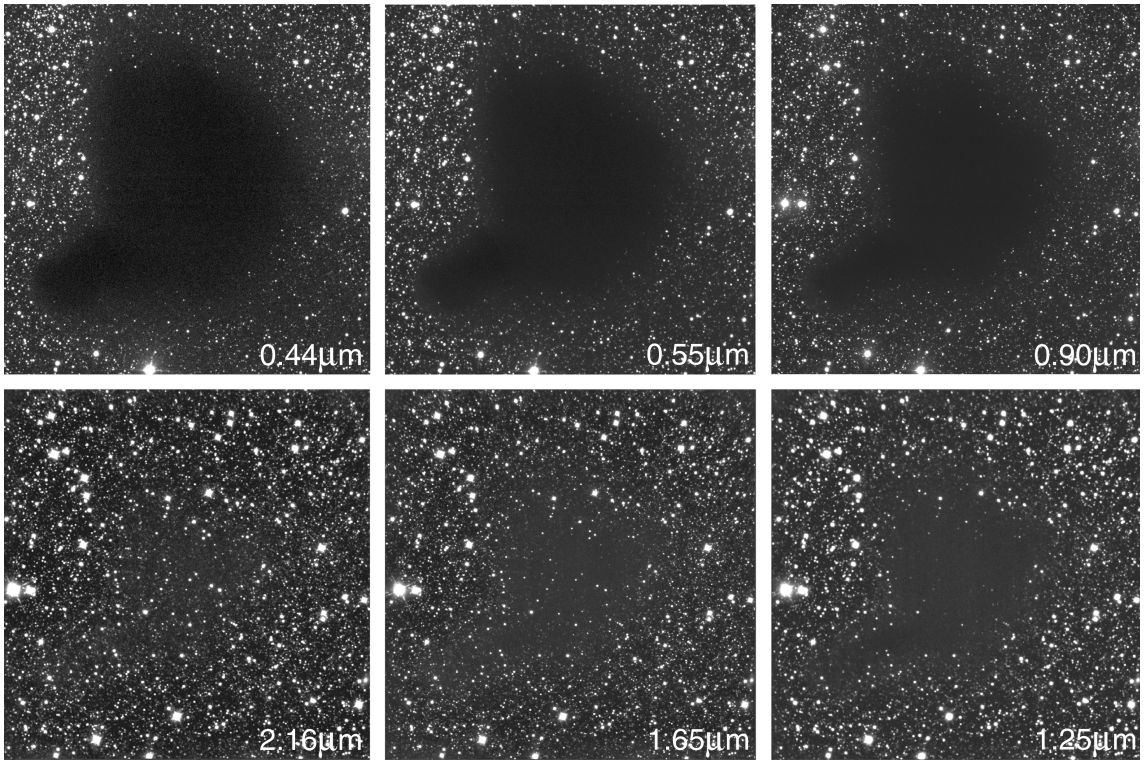

Figure 1.1: Barnard 68 as seen in different (optical to NIR) wavelengths from 0.44 to 2.16 μm. (Alves et al., 2001) The wavelength increases clockwise.

shows an example of a protostellar disk as seen by the Atacama Large Millimeter Array (ALMA)), large infrared surveys are essential in order to understand the fundamental properties of star formation processes. The Visible and Infrared Telescope for Astronomy (VISTA), is especially dedicated to such large surveys. It accompanies the Very Large Telescope (VLT) on a neighboring peak, at ESO's Paranal Observatory. With its 4.1 m primary mirror, 1.65° field of view and sub-arcsec (depending on local seeing conditions) resolution it is both well suited to map large portions of the sky as well as resolving small details Emerson et al. (2006). This makes VISTA the perfect tool for studying the multiplicity properties of the large sample of YSOs in Orion A.

Unfortunately, infrared astronomy, unlike optical or radio astronomy is subject to a number of technical difficulties. The general design of infrared telescopes is usually similar to optical telescopes. However, unlike optical detectors, IR detectors have to be cooled to very low temperatures to avoid incoming radiation from the instrument itself. In addition, IR radiation is strongly affected by absorption through atmospheric water vapor. Ground based IR telescopes therefore need to be built at dry and high altitude locations to avoid at least a portion of the atmospheric effects. The most limiting

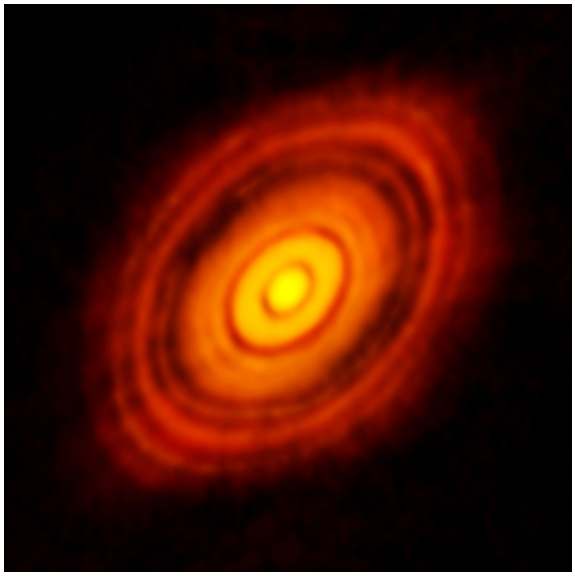

Figure 1.2: Protostellar disk as seen with ALMA (ALMA Partnership et al., 2015), With a resolution of a few tens of microarcseconds, one can even see the dark rings that might have been carved into the dust by newly forming planets.

drawback of IR astronomy is however the cost of IR detectors. Silicate CCDs, as used for optical astronomy are not sensitive to IR radiation. For the low energy photons, other, more expensive materials need to be used. Not surprising, to cope with the higher costs, IR detectors are rarely replaced or repaired. For this reason, the handling of IR data depends upon sophisticated reduction techniques and requires careful examination of potential error sources in the form of image artefacts.

1.2 Young Stellar Objects

Young Stellar Objects (YSOs) are stars that have not yet reached the Main Sequence (MS) of the Hertzsprung Russel Diagram (HRD). Due to their young age, they are (partly) embedded or surrounded by disks of gas and dust, or have just very recently emerged from their parent dust cloud. The surrounding dust imprints itself on the spectral energy distribution (SED) of these young objects.

Figure 1.3 shows some of the SEDs of the first studied protostar cluster in Rho Ophiuchi (Lada and Wilking, 1984). The sources clearly show an infrared (IR) excess, towards longer wavelengths. This peculiar slope of their SEDs distinguishes these IR sources from reddened photospheres of background MS stars. The physical nature of the IR-excess is dust emission of the heated dust envelope/disk that surrounds the YSO.

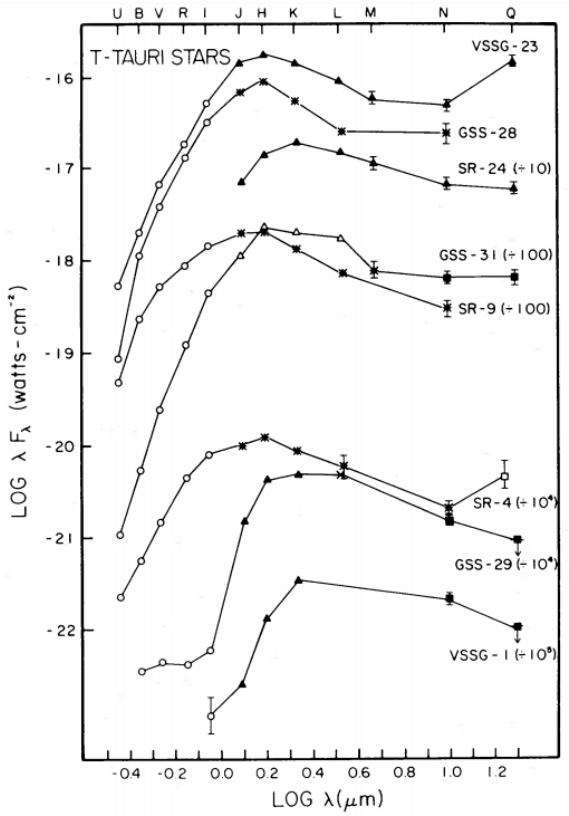

Figure 1.3: Spectral energy distribution for members of the earliest studied protostar cluster (Lada and Wilking, 1984). The IR-excess is clearly visible for all sources, towards the longer wavelengths. The different markers correspond to different sources of photometric data.

First attempts to understand the nature and subsequently classify these objects, were made by e.g. Lada and Wilking (1984); Lada (1987); Greene et al. (1994). Improved observing technologies and the vastly growing amount of available data have largely improved our understanding of the connection between the slope of the SEDs and the evolutionary status of YSOs in the last decades.

One of the resulting conclusions of YSO research is, that the five classes of YSOs, suggested by Greene et al. (1994), indeed represent an evolutionary sequence. The youngest, most embedded Class 0 objects, which are surrounded by an envelope of gas and dust are followed by the still embedded Class I sources with a less prominent, but still dominant envelope. Both of these classes are frequently combined under the term protostars.

The next evolutionary step in the life of a pre-main sequence star is the depletion of the envelope, after which only the surrounding disk is present. For these so-called T-Tauri stars, or Class II sources, the IR excess is not dominating the SED anymore. This shift,

from a dominating IR-excess towards a dominating photosphere is also reflected in the slope of the SED. While the SED shows a positive slope, for a dominant IR-excess, it shows a negative slope for T-Tauri stars. Consequently, there are also YSOs which are identified by a flat SED, with a slope of $\sim$ zero, which represent a transition phase, in-between the protostellar phase, and the Class II phase. These fittingly so-called flat spectrum sources have long had an uncertain status in the evolution sequence of YSOs, but are now confirmed to be an intermediate state, between protostars and disks (e.g. Großschedl et al., 2018b).
And finally, Class III sources present the end of the pre-main sequence evolution. They have almost lost all of their surrounding gas and dust, as well as their IR-excess.
For convenience, and following the naming convention by Großschedl et al. (2018b), in this work, the following synonyms are applicable, in both directions.

- Protostars or P: Class 0 and Class I sources.
- Flats or F: flat spectrum sources
- Disks or D: pre-main sequence stars with disks
- III: Class III sources

In order to fully understand star formation and YSO properties, a large a massive star forming cloud, that hosts a large number of YSOs of all different evolutionary stages, different masses and in different stellar densities is needed. The chances to find such a cloud close to the sun are very slim, or as my supervisor João Alves once said: "We only have one Orion A and there won't be another one anytime soon."

1.3 Orion A - A Massive Stellar Nursery

If you ask anyone outside of astronomy about the star constellations they know, "that big hourglass like one" - Orion - is among the most mentioned, right after the Big Dipper and the "celestial W" - Cassiopeia. For me, when I was a child, I was fascinated with Orion long before I even noticed the Big Dipper or any other star constellations. This gigantic geometrical figure that hovers so impressively over Europe in the winter night sky, made me stare into the sky for hours. When I noticed a small diffuse patch underneath Orion's belt I started puzzling my head about the fascinating unknown worlds that are waiting there to be discovered. Little did I know back then, about the gigantic structures of gas and dust, hiding from our eyes, that accompany Orion's bright stars.

Figure 1.4: Three color image of the galactic western part of Orion A, composed from the VISION JHKs-mosaics (Meingast et al., 2016). The bright Orion Nebula Cluster (ONC) and its surroundings on the right are clearly distinguishable from the more quiescent part of the cloud on the left, where young embedded clusters are visible by their reddish color.

The richest of them all is Orion A. The star forming region extends from the famous Orion Nebula (M 42) in the galactic West, to the bright B star Saiph (κ Orionis) in the Galactic East.

As a prime laboratory for research on the origin of stars, the Orion Molecular Cloud Complex is the richest star forming region near the Sun. It contains a range of different physical environments.

When looking at optical or near-infrared (NIR) maps of Orion A (see for example Figure 1.4), it becomes immediately clear, that Orion A is not a homogeneous cloud, but rather shows a multitude of different substructures. The most prominent and also well studied of which is the Orion Nebula Cluster (ONC, see for example Bally, 2008). In the ONC, the trapezium cluster, in the center of the beautiful H II region M42 hosts massive O, and B stars, some of which are so bright, that they illuminate M42 to the point of naked eye visibility. Similarly, the surroundings of the ONC, along the integral shaped filament (ISF) appear very bright and host relatively massive stars. In the densest, brightest regions, dynamical interactions and feedback from massive stars may have an impact on the formation and evolution of stellar multiplicity. On the other hand, in the

(galactic) eastern part of the cloud, high mass stars are missing. Star clusters in this region, such as L1641, have much lower stellar surface densities. Most of these clusters are still embedded in their birth cloud, and therefore appear reddish. Correspondingly, apart from luminosity and surface density, there are other measurable differences between different parts of the cloud, as shown for example by Meingast et al. (2018).

Großschedl et al. (2018a) divide Orion A into two parts. Motivated by their finding, that Orion A is in fact tilted at a galactic longitude or $\sim 210^{\circ}$, they find, that the cloud has a comet like appearance and call the western part, containing the ONC, the "Head" of the cloud, while the remaining part, east of 210°, is called the "Tail". For simplicity, where applicable, this naming convention is adopted in this work. In order to facilitate comparisons with previous works, a distance of 414 pc (Menten et al., 2007) to the cloud is adopted in this work.
It is, however, indispensable to note that recent findings by Großschedl et al. (2018a) and Kounkel et al. (2018), who estimated the distances to a subset of the YSOs in Orion A with Gaia DR2 data, show evidence, that the assumption of a single distance to the entire Orion A cloud, is not viable. Instead it seems that the Tail of Orion A is tilted away from the observer, with respect to the plane of the sky. The implications of these findings are discussed in Section 4.3.3.

1.4 Stellar multiplicity as a tracer of star formation processes

It is a long known fact, that companion stars can play a crucial role in many astrophysical processes. Supernovae 1A progenitors, for example, are binary systems, companion stars do alter the physical properties of late stages of stellar evolution, by ripping the diffuse outer envelopes of red giants apart, and binary systems are also thought to play a major role in the evolution of star clusters. Very certainly, multiplicity can influence the evolution of protoplanetary disks and therefore the formation of planets and their habitability (Kraus et al., 2016). Numerous conclusions in scientific publications in various fields of astronomical research end with the note, that their results could be biased by an unresolved binary population.Kroupa et al. (1991) for example, show that unresolved binaries have a significant impact on the initial mass function and therefore all results that are drawn from using it. Unfortunately, binary statistics can often not be sufficiently accounted for, partly due to the lack of resolution in binary studies, and partly due to missing statistics. During the past decades, at least MS multiplicity statistics

have reached a high level of confidence (e.g. Duquennoy and Mayor, 1991). The study of young multiples, on the other hand, is still at a quite juvenile state. Considering the observational difficulties discussed in the beginning of this chapter, this is not surprising. Still, in order to understand the processes involved in star formation, it is crucial to get a more complete understanding of multiplicity properties of stars in their earliest evolutionary stages, as they carry the footprints of the mechanisms involved in their formation. While there are numerous attempts to study young multiples, (Petr et al., 1998; Köhler et al., 2006; Kraus and Hillenbrand, 2009, e.g.), these were mostly focused on relatively small populations in distinct environments. Statistically large multiplicity surveys, on an entire star forming region with diverse physical conditions (dense clusters as well as sparsely populated regions) are still the exception.

A full census of the multiplicity status of the YSOs close to the Sun, would be key to understand whether and how stellar multiplicity depends on environmental conditions before and after their formation. Most importantly, it would enable us to answer the questions about the universality of the involved processes and therefore the universality of star formation physics in general.

In order to determine the physical nature of a particular double star, one has to measure the movement of their components around the mutual center of mass. This can be done either by observing the proper motions of the individual components and (at least partially) tracking their orbits, or by spectroscopic measurements. Where the former is possible, and both components are resolved, the binary is called visual binary. Very close binaries, where only the latter method is possible, are called spectroscopic binaries. Two of the most important measures of stellar multiplicity are the companion fraction (CF) (sometimes also called companion frequency) and the multiplicity fraction, or multiplicity frequency (MF) of a certain sample. While the MF gives the fraction of multiple systems within a certain sample, the CF measures the number of companions per primary. The MF and CF for a certain sample only differ, if the multiple systems in the sample are not exclusively binaries but also triples, quadruples or higher order multiples. While the MF of a certain sample can obviously not exceed 100 % (it is impossible that more than all systems are multiple systems), even higher values are possible for the CF (each primary can on average have more than one companion). As mentioned above, the separations between binary components can vary. This is not only important for the observation method, but can also reveal information about the physics involved in their formation and evolution. Looking at the separation distribution of a certain sample of stellar systems is therefore an important tool to learn about the physics of stellar multiplicity. While the true, physical separation of binary stars can only

be calculated, if their orbits are known, Brandeker et al. (2006) find a statistical method to infer the physical separation from the projected separation. In this work, whenever the term separation is used, it refers to the projected separation, if not otherwise mentioned.

1.4.1 Multiplicity on the Main Sequence

Main sequence (MS) stars are much easier to observe than young stars. Unlike YSOs they do not come with the problems of a dusty environment as described in Section 1.1, but equally important, they are much more numerous, as mentioned in the very beginning of this chapter. This is why, in contrast to young stars, we have been having a relatively complete census of MS multiplicity for decades. Duquennoy and Mayor (1991), for example, accomplished a volume limited survey of 164 MS stars within 22 pc. Raghavan et al. (2010) later studied 454 MS stars within 25 pc. Due to the different separation and mass ranges covered in the individual studies of stellar multiples, it is often hard to compare and combine the obtained results. Duchêne and Kraus (2013) give a good overview on the combined status quo on MS multiplicity studies by combining the results obtained for different separation and mass ranges by previous studies. They estimate the CF of solar type MS stars to roughly 62 $\pm$ 3 %. And find a strong correlation of CF numbers with primary mass, yielding a value of of 33 $\pm$ 5 % for masses $<$ 0.5 $M_{\odot}$, while the CF for intermediate to high mass stars reaches 100 % or even higher numbers.

1.4.2 Multiplicity among young stars

As pre-main sequence stars are the progenitors to MS stars, their multiplicity properties should reveal the beginning of the evolutionary path of stellar multiples, which eventually results in the observed MS properties. Reipurth et al. (2014) for example suggest, that all stars might form as stellar multiples, which subsequently decay through the ejection of one component within a hierarchical multiple system. These ejected components are then visible as an excess amount of wide companions with separations larger than $\sim$ 1000 AU. They find strong evidence for a rapid decrease of the number of such wide companions with spectral index (i.e. evolutionary stage), ranging from a fraction of 50 % for the youngest, Class 0 sources to almost 0 % for sources with a spectral index of 0 (i.e. flat spectrum sources). This findings suggest, that these so called soft binaries are subsequently processed via stellar encounters, as is suggested by the Heggie-Hills law, which states, that hard binaries harden, while soft binaries soften in case of a stellar encounter (hard means that the orbital speed of the companion is higher than the speed

of the encounter). While the decay of multiple systems over time is a mechanism that is widely agreed on to play a major role in forming the observed multiplicity properties of MS stars, diverging results for pre-main sequence multiplicity in different star forming regions seem to complicate this theory.

The star forming region that has been best studied early on, in terms of multiplicity, is the region from which T-Tauri stars obtained their name, Taurus-Auriga. Here, Kraus et al. (2011) find that 2/3 to 3/4 of all YSOs are part of multiple systems, when combining measurements over a separation range of 3 to 5000 AU. It is not surprising, that observations of very different star forming regions, such as the ONC, yield different results, since the ejected wide binaries are processed differently. Petr et al. (1998) for example, find that the MF in the Orion Trapezium cluster core matches the observed low values for MS stars very well. The comparison of these results with the roughly twice as high values obtained for Taurus seem to favour the theory, that initially all stars are formed in multiple systems, which are later disrupted, due to dynamical processes. In order to prove this general idea, Köhler et al. (2006) compare the findings of Petr et al. (1998) with their own results for the periphery of the ONC, where stellar densities are much lower and comparable to the Taurus star forming region. Surprisingly, they find that their results are comparable to that obtained by Petr et al. (1998). Their obtained MF numbers are only non significantly higher then that for the ONC. This finding leads them to the conclusion, that in fact, binary formation is dependent on environmental properties. On the other hand, recent high resolution studies of stellar multiples in the ONC by Duchêne et al. (2018) yield a CF of $\sim$ 21 % for a separation range of 10 to 60 AU. This value is twice as high as the value for MS stars and consistent with other star forming regions. Their findings lead them to the conclusion, that binary formation is indeed initially universal over all environments, and subsequently altered. However, their finding shows, that the combined results of multiplicity properties in different star forming regions can not explain the observations of the MS properties, since the low CF for MS stars can not be a result of the mixture, or the processing of the observed pre-main sequence population. Further, the nature of the relatively low amount of wide binaries found by Köhler et al. (2006), still lacks a satisfying explanation.

In an attempt to better understand the overall properties of stellar multiples in those star forming regions of Orion, which are not part of the dense ONC, Kounkel et al. (2016) conducted a multiplicity study of 354 YSOs in Orion A and B. Their results are somewhat surprising. With a CF of $\sim$ 14.4 % for protostars, and $\sim$ 12.5 % for pre-main sequence stars with disks, at separations between 100 and 1000 AU, they do not find a significantly different CF for neither, different evolutionary stages of YSOs, nor the

estimates for MS stars and the YSOs in their sample. They argue, that this might be due to the fact, that their observed sample is biased towards YSOs where the decay of multiple systems has already occurred. Further, they find a 50 % higher CF for their sub-sample with higher YSO surface density, when compared to the remaining YSOs. This result is somewhat puzzling when compared to the overall consensus of possible formation and evolution scenarios for stellar multiples. Kounkel et al. (2016) state, that their finding suggests, that either their higher density sample is biased towards higher luminosity, i.e. higher mass stars (which they however consider as unlikely) or is an imprint of an enhanced formation of multiple systems in regions with higher densities.
The overall conclusion of the above mentioned status quo of young multiplicity is, that either Orion just does not obey the "rules" or we are still missing some fundamental information of the formation and evolution of stellar multiples. In any case, in order to disentangle the remaining ambiguities, further work is needed, ideally including a complete sample of the YSOs in Orion across all different environments and ages, and yielding high quality statistics. Consequently, the aim of this work is to develop an Automated COmpanion DEtection Routine (ACODER), in order to investigate the multiplicity properties of the largest sample of young visual binaries to date, consisting of the $\sim$ 3000 YSOs in Orion A.

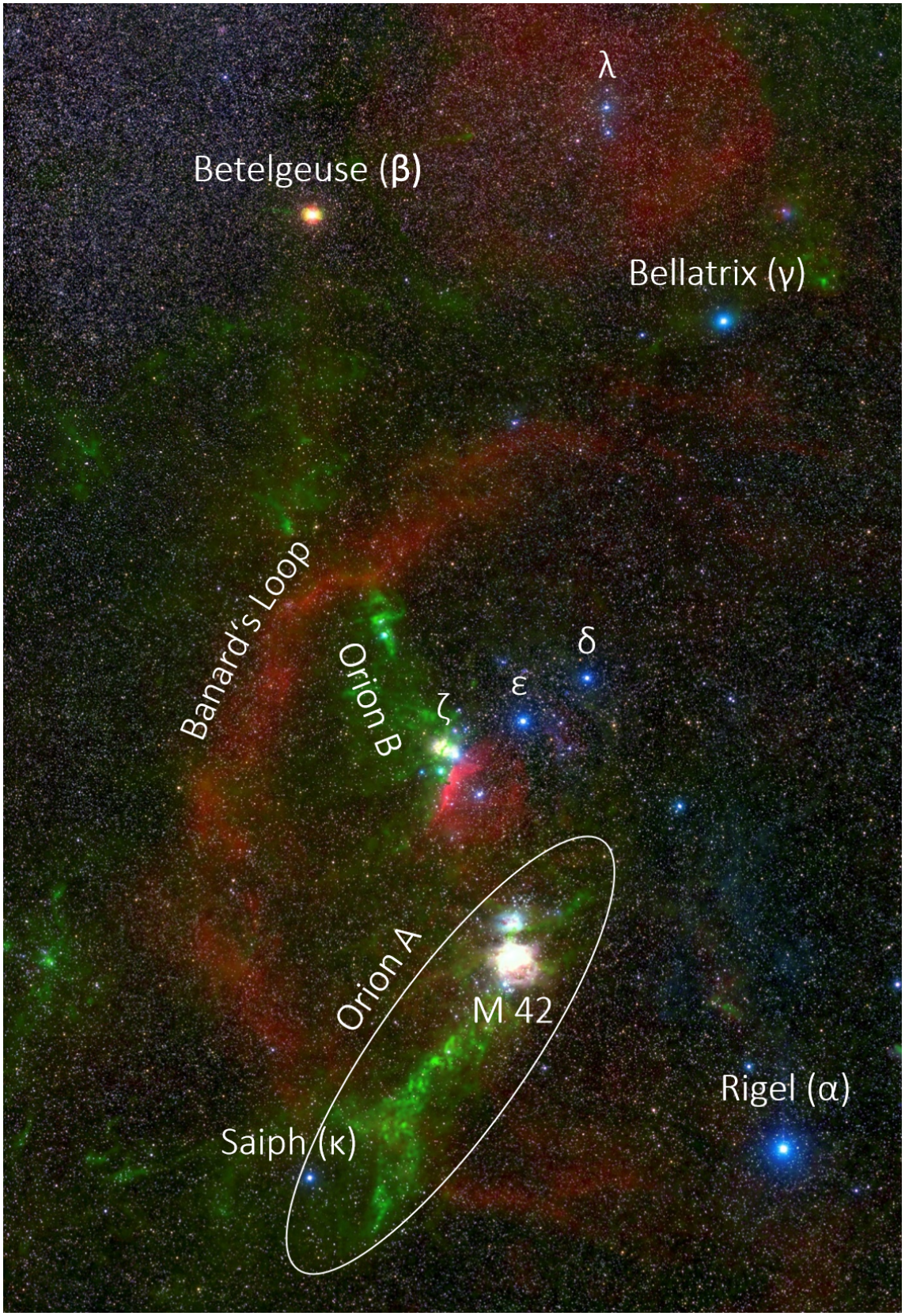

Figure 1.5: Overview of the Orion constellation and the most prominent stars and structures therein. NIR extinction map (green): Lombardi et al. (2011) Optical: Wei-Hao Wang, IfA, University of Hawaii.

Chapter 2

Data

The original image data for this study is mainly taken from the Vienna Survey in Orion - VISION (see Section 2.1 & Meingast et al., 2016). The survey catalog contains almost 800,000 sources among which are the well known Orion Nebula Cluster (ONC), as well a few thousand Young Stellar Objects located in very different environments, such as isolated star forming regions as well as embedded and dense clusters. The Young Stellar Objects in the Orion A molecular cloud have been subject to many studies, e.g. Megeath et al. (2012), Megeath et al. (2016), Pillitteri et al. (2013), and have recently been revisited by Großschedl et al. (2018b). Großschedl et al. (2018b) is the most complete and up-to-date catalog of Orion A YSOs, as well as the largest catalog of YSOs towards one single star forming region. As a training sample, for the development of a reliable companion detection routine, I used the data on 335 YSOs in Orion A, that have previously been studied by Kounkel et al. (2016) using Hubble data. These data are described in Section 2.2.3

2.1 Image data: VISION

The Vienna Survey in Orion (VISION, Meingast et al., 2016) was carried out with the ESO Visible and Infrared Survey Telescope for Astronomy - VISTA (Sutherland et al., 2015). Starting in October 2012, almost the entire Orion A cloud was observed within six months, covering an area covering of ~ 18.3 deg^2 on the sky. The survey provides high-quality, sub-arcsec, seeing limited images for 799,995 sources. The central wavelengths for the J, H, and Ks bands are 1.22 μm, 1.63 μm, and 2.19 μm respectively. The corresponding magnitude limits are 20.4, 19.9, and 19.0 mag (at the 90 % completeness limit). The seeing limited resolution of VISTA of about 0.8 arcsec, theoretically enables

to resolve binary separations larger than 330 AU (at a distance of 414 pc, Menten et al., 2007).

2.1.1 Subimages

One of the most crucial steps for the detection of faint companions is proper point spread function (PSF) fitting. The shape and quality of a source's PSF is however largely influenced by the seeing conditions at the time of observation. Due to the large field covered by VISION, the observations were spread over several months. The seeing therefore varies across the whole mosaic. Further, to account for gaps between the single detectors (see Meingast et al., 2016), the number of observations is not equal for every sub-region. Figure 2.1 shows the Ks-band seeing map of the entire VISION mosaic as an example. Regions with relatively constant seeing roughly correspond to the size of a VIRCAM (VISTA) detector of $\sim 10.6 \times 10.6$ arcmin.

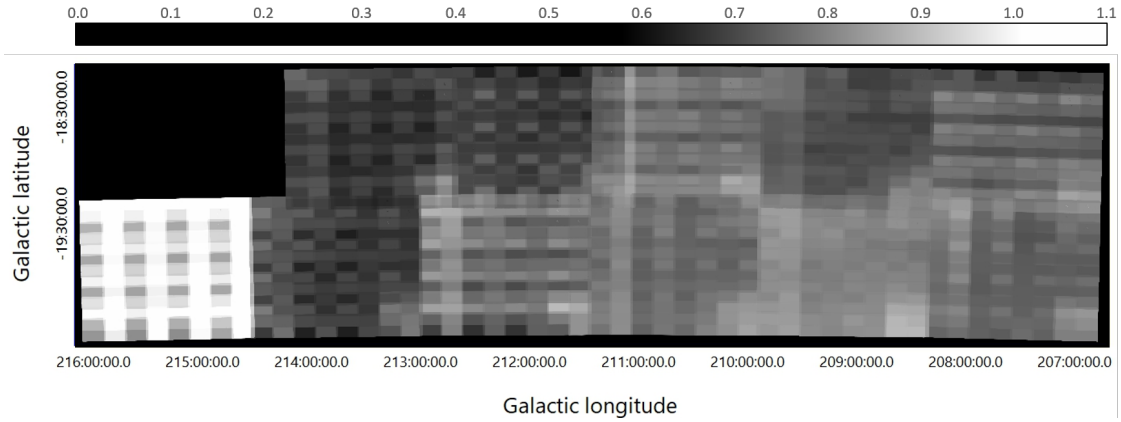

Figure 2.1: Seeing map in Ks-band for the entire VISION mosaic

In order to produce reliable PSF models for sources across the entire VISION field, seeing variations among such stars that contribute to the PSF model (PSF contributors) need to be kept at a minimum. For the automated routine, an easy and efficient method to do so, is to separately analyze sub-images of sizes that correspond to the VIRCAM detector size. Using even smaller sub-images, would have a positive effect on eliminating seeing variations, but would on the other hand lead to a lack of input sources for PSF modeling. The development of more sophisticated methods for the handling of seeing variations is part of future refinements of ACODER (see Section 6). The local seeing conditions for each target source is found in the VISION catalog. The mean seeing for the whole Orion A survey is 0.78, 0.75, 0.8 arcsec for J, H and Ks, respectively.

2.2 YSO catalogs

The Großschedl et al. (2018b) YSO catalog, hereafter called G18, is the most up-to-date catalog of YSOs in Orion A. The 2980 catalog YSOs with infrared excess are classified by revisiting and extending previously available YSO catalogs in Orion A (e.g. Megeath et al., 2012, 2016). For their YSO analysis, G18 use VISION data, as well as archival Spitzer and Wise data. They find 274 previously unknown YSO candidates and remove $\sim$ 5 % false positives or uncertain sources from archival catalogs. Using extinction corrected spectral indices, they classify the newly identified YSOs, and reclassify some of the previously known sources. The resulting YSO catalog contains 60 Class 0 protostars, 128 Class I protostars, 185 flat spectrum sources, and 2607 pre-main-sequence stars with disks, as seen in Table 2.1.

The YSOs found in G18 are distributed over the entire Orion A cloud, an area of $\sim$ 18.3 deg^2 and do not only cover different evolutionary stages, but also a range of different physical environments, from well known dense clusters to isolated (Taurus-like) star forming events towards the southern end of Orion A. This unique sample of YSOs offers a great opportunity to seek the answers of many questions related to star formation. In the case of this study, it enables us to directly compare the multiplicity status of young stars found in different environments and at different evolutionary stages. As an example, some of the sources found in G18 are shown in Figure 2.2. One can already distinguish between the red and embedded and the bluish more evolved sources by eye. Also, some of the sources clearly are multiples.

Table 2.1: Number counts of different YSO classes found in G18 (1) and P13 (2).

YSO Class	Number count
Class 0 (1)	60
Class I (1)	128
Flat spectrum sources (1)	185
Pre-main-sequence stars (1)	2607
Class III sources (2)	495

Pillitteri et al. (2013) carried out an XMM-Newton survey along L1641 and the iota Orionis region. They compile a catalog of 495 sources with high x-ray luminosity but a corresponding normal photospheric appearance in the mid-IR and classify them as Class III YSOs, which are already more evolved than the sources found in G18. This catalog is hereafter called P13. In order to achieve even better insights into the evolution of multiplicity over time, these more evolved sources are a useful addition for the target

Figure 2.2: Selected sample of YSOs from the Großschedl et al. (2018b) sample (Großschedl et al., 2018b, Fig.A.2). The number is the ID in their catalog, the letter in brackets to the right is the YSO class. The letter to the left indicates their alphabetic order of these selected YSOs.

catalog of this study.

2.2.1 Initial target catalog (ITC)

The 2981 G18 sources as well as the 495 P13 sources were cross-matched with the VISION catalog. 2931 of the G18 YSOs have a counterpart in the VISION catalog, as well as 470 P13 Class III sources. Some of the sources in the VISION catalog are found in both, the G18 and the Pillitteri et al. (2013) catalog. In some of these cases, they have different YSO classes assigned to them in the two catalogs. In such cases, the classification by G18 was given priority, since their SED analysis as well as the data used for their study was more extensive. The combined catalog, hereafter called ITC (initial target catalog), contains 3386 sources with evolutionary stages from Class I protostars and flat spectrum sources to pre-main sequence stars with disks and Class III objects

Table 2.2: YSO counts in the ITC.

YSO Class	Number of stars
Protostars	143
Flat spectrum sources	181
Pre-main-sequence stars with disks	2607
Class III sources	455

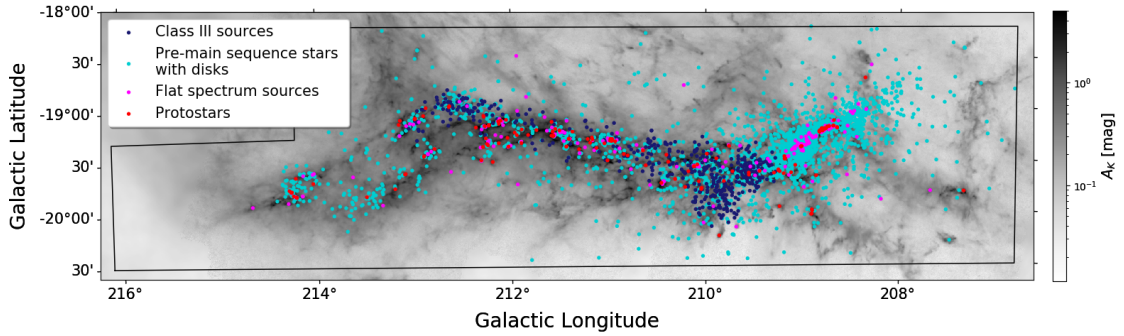

Figure 2.3: Distribution of all YSOs in the initial target catalog (ITC). Gray shaded background: Planck-Herschel-Extinction dust column-density map (Lombardi et al., 2014). The black line marks the borders of the VISION field. The colored dots mark the locations of different classes of YSOs: dark-blue: Class III sources, light - blue: pre-main sequence stars with disks, magenta: flat spectrum sources, red: protostars.

without disks. The number counts for the different YSO classes in the ITC are listed in Table 2.2, and their distribution on the sky is shown in Figure 2.3.

Unfortunately, due to insufficient data quality, as a result of saturation or crowded areas, for part of the ITC sample, a companion detection is impossible at the scope of this work. Treating the affected sources equally as those which are not affected, might introduce unacceptable errors to the result. They have therefore been excluded from the current analysis and will be subject to following studies. The selection of these sources is described in the following section.

2.2.2 Exclusion of potential error sources

In order to avoid introducing errors to the final result, a relatively conservative selection of potential error sources has been made.

Saturated sources

Some preliminary ACODER test runs showed that for saturated stars the results strongly differ from the expected outcome. The reason for this is that the PSF of a saturated single star, does not show a well defined central peak on the VISTA images, but rather consists of a ring of smaller peaks surrounding a central hole (see Fig.2.4a). This specific behaviour is induced by the typical two-step readout process of IR detectors, conducted also by VIRCAM on VISTA (Sutherland et al., 2015). When trying to fit the PSF of such a star, more than one peak is detected, hence the subtraction fails and in the subsequent source detection, the residuals introduced by the wrong fitting process are detected as false companions. Even though the detection of too many companions is suspicious and would lead to the target being flagged for further examination, this might not be the case for targets which are only moderately saturated, as shown in Figure 2.4b.

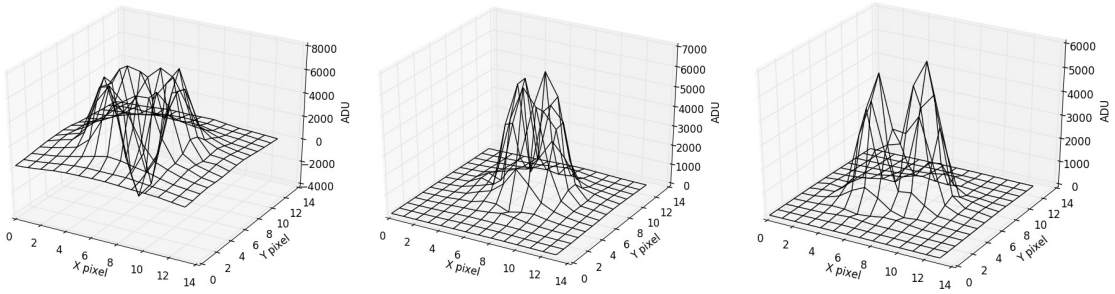

(a) Saturated star. **(b)** Moderately saturated star. **(c)** Binary.

Figure 2.4: Surface plot of a saturated star (a), a moderately saturated star (b) and a binary (c). If saturated stars are not treated carefully, especially moderately saturated stars can easily be confused with binaries.

It is important that all possibly saturated targets are flagged prior to the fitting process, for reasons described above. To ensure this, a quite conservative approach was chosen and the non-linearity magnitude limits of 13, 12 and 11.5 for J, H and Ks band respectively, estimated by Meingast et al. (2016) were applied. These values were obtained through a comparison of the VISTA magnitudes with their 2MASS counterparts (if available). In this way, 1267, 1238, and 1295 sources in J, H and Ks band respectively, were flagged as saturated and subsequently automatically excluded from the ACODER analysis.

For many saturated objects, an analysis in the complimentary bands leads to better results and still makes a companion detection possible. 61 targets, however, are saturated in all three bands and will therefore likely fail all PSF fitting attempts. For these objects, follow-up observations were carried out with the NACO instrument on VLT UT1 in period 100 (see Section 6)

Faint objects

Besides the saturated sources, some of the ITC sources are located on the other extreme of the brightness range. These are too faint to be found with a reasonable detection threshold, which still prevents the detection of spurious sources. ITC YSOs with a peak flux smaller than 10 ADU are flagged as "too faint". For most of these sources, however, this is only true in one of the bands and an analysis is still possible in the complementary bands. Where this is not the case, the analysis can be carried out manually (see Section 6).

The edges of VISION

Some of the targets are located too close to the edges of the VISION field to find enough stars for PSF modeling, in a cutout centered on the target. These sources were flagged. In order to include them in the analysis, their cutout field needs to be re-centered. This should also be accomplished automatically by ACODER in the future.

Crowded areas

Due to high sky background noise, the automated companion detection routine is likely to deliver numerous false positives within crowded areas, such as the ONC. In order to flag the affected sources, the background noise was estimated using an iterative 3-sigma clipping python algorithm, which was provided by Stefan Meingast (personal communication). The average sky background noise was determined within a 200 x 200 pixel square, centered on each individual source in the ITC sample. Wherever the target is located too close to the edge of the mosaic, the square was shifted accordingly. The background noise information was stored in the ITC and used also as an input for the subsequent ACODER analysis. Figure 2.5 shows the distribution of the sky background noise over Orion A. Regions with high values correspond to the densest parts of Orion A. A limit of 2 ADU on the background noise seemed to map the most crowded regions best, consequently YSOs with exceeding noise are flagged as "crowded". As these targets are the most likely to yield erroneous results they are excluded from the current analysis.

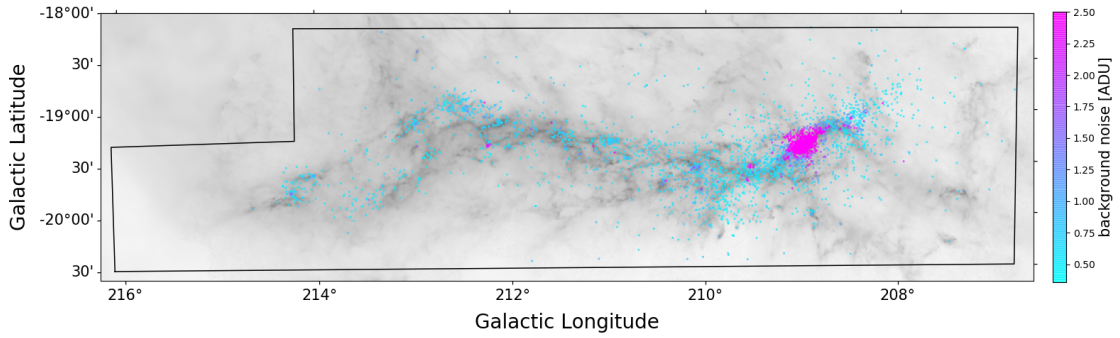

Figure 2.5: Sky background noise for YSOs in the initial target catalog (ITC). Gray shaded background: Planck-Herschel-Extinction dust column-density map (Lombardi et al., 2014). Colored dots: YSO positions in Orion A and their sky background level (in ADU) in a 200 · 200 pixel box around the YSOs (color coded). Magenta colors correspond to the regions with highest background noise.

Table 2.3 shows the numbers of sources affected by the above mentioned issues. However, some of these sources do suffer from more than one issue, leaving the total number of excluded sources well below the sum of sources affected by the different issues. 1692 J-band, 1689 H-band and 1686 Ks-band targets passed the selection criteria, leaving a total of 1965 targets. ACODER automatically sorts through all sources of the ITC, moves their corresponding images to a different folder and proceeds with the analysis on the resuced target catalog, containing only sources that passed all selection criteria.

Table 2.3: Sources that have been removed from the ITC due to issues discussed in Section 2.2.2.

Issue	J-band	H-band	Ks-band
saturated	1267	1238	1295
too faint	91	49	22
edge	25	25	25
crowded	613	755	781
all	1694	1697	1700
remaining	1692	1689	1686

2.2.3 Training sample

For the purpose of testing and refining the companion detection routine (see Section 3), a training sample of well studied multiples and singles in Orion A was needed.
Kounkel et al. (2016) observed 399 selected YSOs, taken from the Megeath et al. (2012) catalog, in Orion A and B. 335 of them lie within the VISION field. While their sample size is small, compared to this work, they used the Hubble Space Telescope (HST) for their observations and consequently their data has a much higher resolution. They observe multiples with separations down to 0.24 arcsec (100 AU at a distance of 414 pc). This means that the multiples which are found in both, the ITC (lower VISTA resolution), and the sample studied by Kounkel et al. (2016), should be well resolved in their HST image data. Hence, the Kounkel et al. (2016) sample is well suited to serve as a resource to analyze the capabilities and completeness limits of the method used in this work (see Section 4.2). Out of their 354 targets, 335 are located in Orion A. Kounkel et al. (2016) find that 45 of them have at least one companion within 2.4 arcsec (1000 AU), while the remaining 290 YSOs are single.
239 and 35 of these single and multiple sources are found to have a counterpart in the VISION catalog. These, in total 274 sources are hereafter called the training sample.

Chapter 3

Methods

For the identification of close companions towards the target YSOs, multiple instances of photometric analysis, source detection, PSF fitting and subtraction had to be carried out for each source in the ITC. The large sample size of 3565 sources, necessitated the automation of these processes while the exclusion of potential false positives in the form of spurious sources or residuals from PSF subtraction processes was of highest priority. To accomplish this task, I developed ACODER, an Automated COmpanion DEtection Routine. ACODER is a Python/PyRAF based routine and was designed to complete the following tasks for each individual target and all three bands:

- VISION-cutouts (Section 3.1)
- Source detection on original VISION-cutout (Section 3.2)
- Measurements on detected sources and target determination (Section 3.3)
- Selection of suitable PSF model contributors (Section 3.4)
- Computation of the PSF model, fitting and subtraction on original VISION-cutout (Section 3.5)
- Source detection, PSF fitting and subtraction on subtracted image (Section 3.6)

Finally, the results are combined for all targets in all three bands (Section 3.8) and the subset of reliable source detections is defined (Section 3.8.2). The subsequent determination of the number of bona fide companions is accomplished using a statistical method (Section 3.9). Since the image data used in this study do not provide any information on orbital parameters (e.g. spectra, proper motions), it is impossible to directly determine the physical multiplicity status of a certain system. An identified binary system,

without any further information, could simply be a projection coincidence. However, within a statistically large sample, the likelihood of such a projection coincidence can be well determined, allowing to infer the overall amount of companions towards the sample. Consequently, in this work, all projected neighbors to a target source are referred to as companion candidates (CCs), as their true nature can not be determined.

In this section, I describe the individual tasks of ACODER, some complications on the way to find CCs, as well as the statistical approach for the determination of the number of bona fide companions. The most important fixed input parameters for ACODER are listed in table 3.1. These parameters where chosen as a result of a series of test-runs on the training sample and subsequent visual examination. Other parameters are individually estimated for each target by ACODER, as described in the following sections.

Table 3.1: Fixed PyRAF input parameters used in ACODER.

Name	IRAF task	Value	Unit
datamax[1]	datapars	3000, 6000, 6000	ADU
sigma	datapars	individual	ADU
thresho	findpars	10	sigma
fwhmpsf	datapars	individual	pixels
functio	daopars	auto	
varorde	daopars	2	
psfrad	daopars	15	pixel
fitrad	daopars	15, 2.5	pixels
sannulu	daopars	10	pixels
wannulu	daopars	11	pixels
apertur	photpars	5	pixels
maxnpsf	pstselect	100	

[1] for J, H and Ks respectively

3.1 VISION-cutouts

For each source in the ITC, and all 3 bands, a 10.6 x 10.6 arcmin sub-image was cut out of the VISION mosaic. ACODER uses montage-wrapper, a Python module for the IPAC Montage mosaic software[1] to accomplish this task, as it is easy to script and to combine with subsequent data heavy tasks. To ensure projection type compatibility with

[1]Montage is funded by the National Science Foundation under Grant Number ACI-1440620, and was previously funded by the National Aeronautics and Space Administration's Earth Science Technology Office, Computation Technologies Project, under Cooperative Agreement Number NCC5-626 between NASA and the California Institute of Technology."

IRAF/Pyraf, all sub-images are re-sampled, afterwards. For this purpose ACODER uses the Astromatic software package SWarp, again, because it is easily scriptable which is critical as there are a few thousand images to be processed. The resampling process also involves the production of 3565 sub-images from the VISION weight maps in each of the three bands for each target. In sum, the above described data preparation steps alone produced $\sim$ 50,000 individual images for the analysis of the thousands of YSOs. This makes clear, that the some of the main problems I had to deal with, were data storage, proper naming and archiving and automation. Even commonly simple tasks, such as sorting or renaming needed to be carefully scripted. During this part of the ACODER routine, all images that correspond to targets that have been flagged as potential error sources (as described in Section 2.2.2) are moved to separate folders, where they are available for future analysis (see Section6.2).

3.2 Source detection on original VISION-cutouts

Different source detection and PSF modeling tools (SExtractor, PSFEx and IRAF-daophot) were tested in order to find the best possible strategy for the data and YSO sample analyzed in this work. A comparison of the results for the training sample (described in Section 2.2.3) with the literature (Kounkel et al., 2016) was used as a measure of success. The generation of satisfying results with automated methods at hand (SExtractor, PSFEx) was difficult. While these methods work very efficiently on large data sets, the accuracy of the PSF fitting process was not sufficient for the detection of faint and relatively close CCs. A manual fitting process with IRAF-daophot and hand-picked PSF contributors on the other hand quickly lead to much better results. Since IRAF is not designed for an automated use on large data sets, the preferred tool for ACODER became a python implementation of IRAF, called PyRAF[2]. The goal of the PSF contributor selection became the closest possible imitation of the successful manual test runs.

The source detection itself is accomplished, using the PyRAF task daofind, with a detection threshold of 10 σ, where σ is the local sky background level (determined as described in Section 2.2.2), which is read out from the ITC for each individual target and band. The parameter datamax, which is read out by daofind from the datapars file, is the maximum allowed pixel value in ADU and corresponds to the non-linearity limit. Sources which contain pixels with values above datamax are excluded from the analysis.

[2]PyRAF is a product of the Space Telescope Science Institute, which is operated by AURA for NASA

In order to estimate the non-linearity limit in ADU for each band, the peak flux in ADU is plotted against the VISION-magnitudes for each target and band in Figure 3.1. The peak flux was determined within a 10 x 10 pixel area around each target. The black cross in the plots mark the the non-linearity magnitudes of 13, 12 and 11.5 for J, H and Ks respectively. Datamax was accordingly set to 3000, 6000 and 6000 ADU respectively.

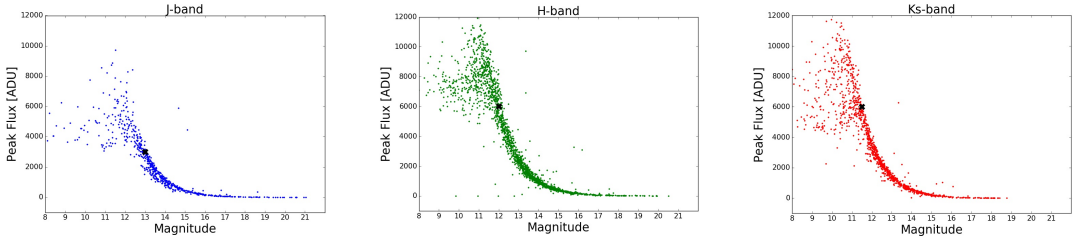

(a) J-band. **(b)** H-band. **(c)** Ks-band.

Figure 3.1: Peak flux in ADU plotted against the magnitudes in a) J-band, b) H-band and c) Ks-band. The black cross marks the non-linearity magnitude given in Meingast et al. (2016).

Another important input parameter for daofind is the expected full width half maximum (fwhmpsf) which corresponds to the seeing. As described in Section 2.1.1, the seeing is not constant over the VISION mosaic and needs to be read out from the VISION catalog for each individual sub-image.

3.3 Measurements on detected sources and target determination

In order to reliably subtract the target PSFs (see Section 3.5), the development of a good PSF model is key. Due to the observation method and instrumental setup (see Section 2.1), PSF models need to be calculated for each individual sub-image. The goal of the subsequent PSF subtraction is to optimize the fitting of the target source, rather than the remaining sources on a sub-image. Hence, the routine was designed as such, that it only allows sources as an input for the PSF model, that are of similar magnitude as the target while otherwise representative for an average and "well behaved" source in the sub-image. Before picking these sources, some additional measurements needed to be carried out on each source and the target itself needs to be determined. The magnitude of each source was determined via aperture photometry using the PyRAF task phot. The aperture radius was set to 5 pixels and the inner radius of the sky fitting annulus as well as its width were set to 10 pixels. In addition the FWHM has to be determined in order to decide about the suitability of a source as PSF contributor. This can be

achieved using the non-interactive mode of the PyRAF task imexamine. Unfortunately, this method of determining the FWHM is extremely computationally expensive as it is not designed to be used for a large number of sources or images. A much faster way to accomplish the task of measuring the FWHM was provided through an R script by Francisco Surot Madrid (personal communication). The inclusion of this script into my routine resulted in a reduction of computing time to 5 % of the initial computing time.

The coordinates of the target YSOs are theoretically known from the VISION catalog, and the sub-images are centered on these coordinates. However, some of the targets are of course binaries or higher order multiples, and some of them show extended emissions or outflows. As a result, for some of the targets, the VISION coordinates do not belong to a single source but are located somewhere in-between multiple stars or in the center of an extended emission. ACODER, however, does mostly detect the actual sources that make up such a system, and the coordinates then do not match the VISION coordinates. Figure 3.2 shows an example for such a case.

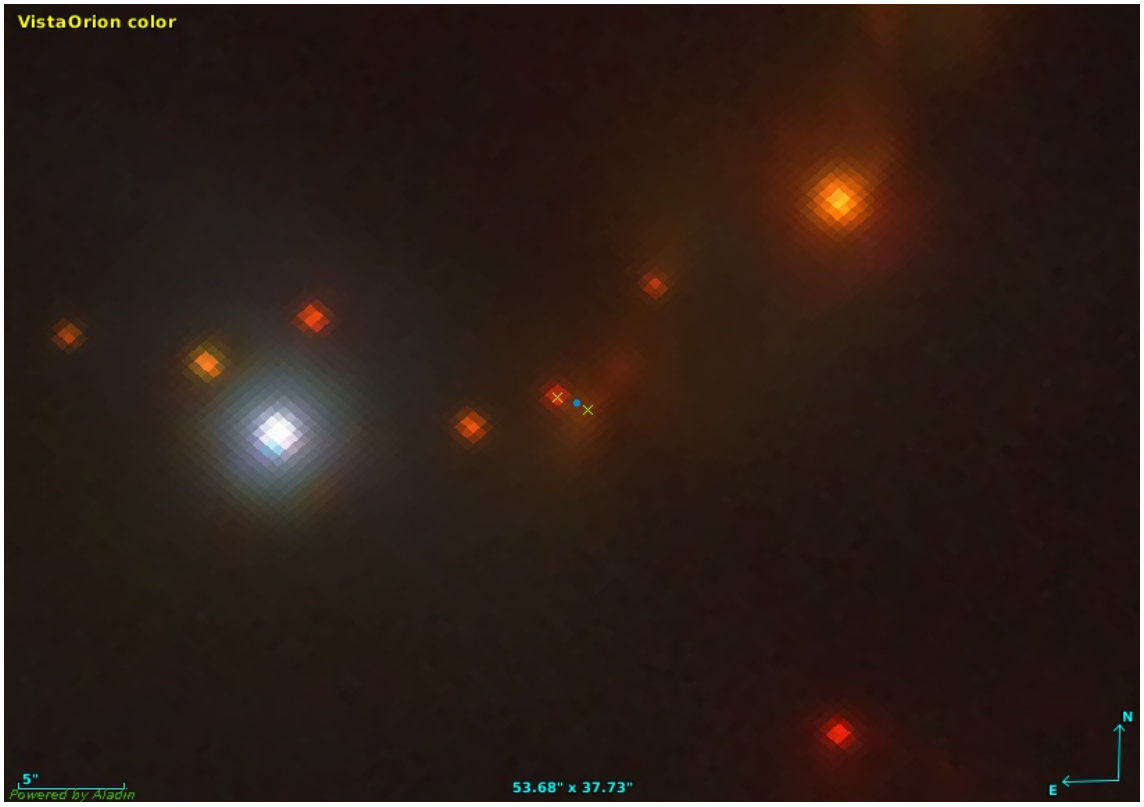

Figure 3.2: Three color VISTA image of a case where the target coordinate in the VISION catalog (blue dot) differs from the coordinates found by daofind (green crosses).

In order to identify the actual target in such a case, the original VISION coordinates are automatically converted into image coordinates, by reading out the image header

information. All sources found within a radius of 3 pixels $\sim$ 1 arcsec) from the original target coordinates in the VISION catalog are compared, and the brightest of them is considered the actual target.

3.4 Selection of suitable PSF model contributors

The magnitudes and FWHM (measured as described in the previous section) as well as some information on the shape characteristics found in the daofind output files and the distance to the target are used to select stars as PSF contributors. The restrictions on these properties were determined by the comparison with sources that lead to good results in multiple manual test runs. The following restrictions need to be satisfied by PSF contributors:

- The sharpness (see PyRAF manual: daofind for explanation) lies within a range of $\pm$ 0.6 σ of the median sharpness of the sub-image.
- The roundness (see PyRAF manual: daofind for explanation) lies within a range of $\pm$ 0.6 σ for ground and $\pm$ 1.5 σ for sround of the median roundness of the sub-image.
- The FWHM lies within a range of $\pm$ 1.2 σ of the median FWHM of the sub-image.
- The magnitude of the source is similar to the target in a range of $+3$ and -1 mag, in order to exclude saturated stars, and $+2$ and -2 mag for stars fainter than 17^{th} mag in order to choose, where possible, stars above a 20 σ limit, which, in most cases, roughly corresponds to a magnitude of 20.
- The target itself is not allowed as PSF contributor to avoid biases in case it actually is a binary. This is ensured by an avoidance radius of 10 pixels around the target.

In addition, the PyRAF task pstselect is used to filter out sources with brighter neighbors or close to the image edges. The allowed distance to bright neighbors or the image edges is set by the parameters psfrad and fitrad, which were both set to 15 pixels for this part of the routine (For more information on pstselect, see IRAF manual - pstselect). The maximum number of selected PSF stars was set to 100.

Finally, in order to be accepted as PSF contributor, a source has to satisfy both the selection criteria of pstselect as well as the other restrictions described in this section.

3.5 PSF modeling, fitting, and subtraction on original VISION-cutout

With the list of PSF contributors (obtained as described in the previous section) as an input, a PSF model is created for each individual sub-image, using the PyRAF task psf. Using the PyRAF task allstar, the model is then subtracted from all sources that have been detected via daofind in the previous steps. The parameter fitrad (used by pstselect previously) is used by allstar as well and needs to be changed to a smaller value, similar to the FWHM before executing allstar. The coordinates of all successfully subtracted stars are separately stored in a file. Figure 3.3 shows an example of an output image after the PSF subtraction.

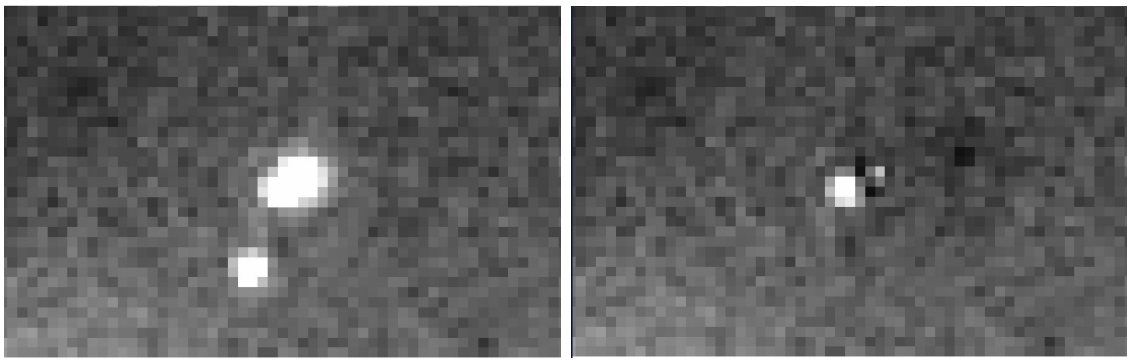

(a) Target 05352785-0505362 before subtraction. **(b)** Target 05352785-0505362 after subtraction.

Figure 3.3: Example of successful PSF subtraction: The two images show the same target before (a) and after (b) subtraction. The source at the bottom was completely subtracted. For the upper source only the primary was subtracted, while the secondary is left.

Unfortunately, the VISTA images suffer from undersampling. Due to the excellent seeing (down to 0.6 arcsec), the average full width at half maximum (FWHM) of the PSFs can go down below 2 pixels, due to the comparably large pixel size of 0.34 arcsec (Sutherland et al., 2015). The imaged PSFs therefore do not show well-behaved Gaussian profiles, but are instead rather peaky. (see Figure 3.4). This special shape is difficult to model with PSF fitting tools, leading to residual artifacts especially at the position of the peak. As a possible solution, the opportunity of smoothing the images prior to the PSF fitting process, was considered. Using the PyRAF task boxcar, with a 3 x 3 pixel kernel, smoothed images were produced and processed and analyzed as described in Section 3.8.2. The smoothed PSF profile (see Figure 3.5) is indeed easier to fit. The analysis of the results for the training sample, however, shows that on the other hand, the loss of resolution affects the detection of faint and close companion candidates

negatively. I therefore decided to work with the original VISTA PSFs instead.

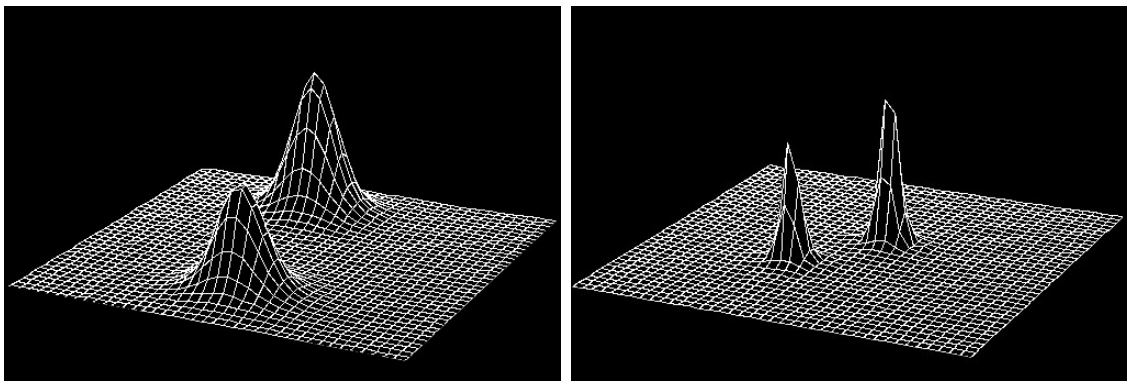

(a) Gaussian PSF. **(b)** VISTA PSF.

Figure 3.4: Comparison of a well behaved gaussian PSF (left panel) and a typical VISTA PSF under good seeing conditions (right panel).

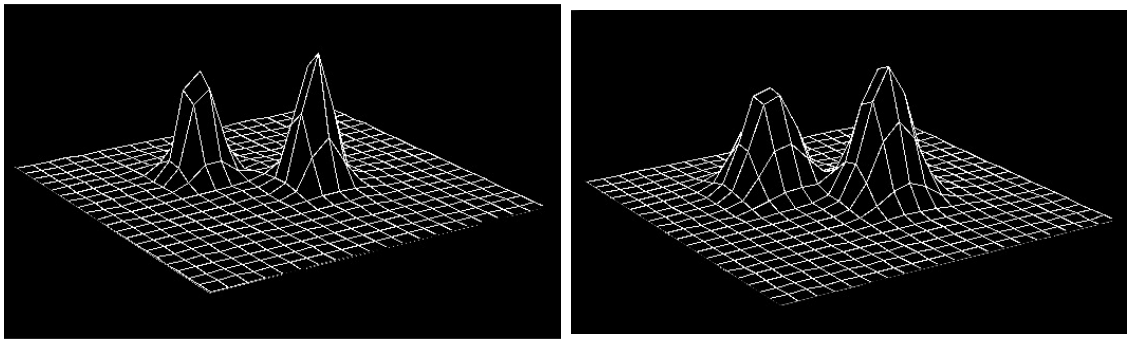

(a) Original VISTA PSFs. **(b)** Smoothed PSFs.

Figure 3.5: Binary with original VISTA PSF and typical peaky profile (a), the same stars smoothed with PyRAF-boxcar, using a 3 x 3 pixel kernel (b).

3.6 Source detection, PSF fitting and subtraction on subtracted image

On the central area of the subtracted image, another run of PyRAF daofind and phot is executed, using the same parameters as in the first run. For this part of the routine, instead of the whole image, a smaller, 120 $\times$ 120 pixel ($\sim$ 41 arcsec) sub-image, centered on the target position was used as an input for daofind and phot, to concentrate on the target's neighbors. The detected sources are used as an input for an automated run of the PyRAF task imexamine. Imexamine provides three different measures for the

FWHM (see PyRAF manual: imexamine for further information) as well as the flux and peak count in ADU. With such a limited number of sources, using imexamine is not problematic anymore, since the number of sources is much smaller than in the first part of the routine. In addition, to get a larger set of properties of all detected sources for later analysis, the R script for the determination of the FWHM is used to extract an additional measure of the FWHM of these sources. Finally, in order to test if the PSFs of the newly detected sources are of such shape that they can be fit with the previously created model (see Section 3.5), another run of allstar is carried out on these sources. The sources which were successfully subtracted are stored in another output file, which can be used for the analysis of the CCs quality.

3.7 Photometric Calibration

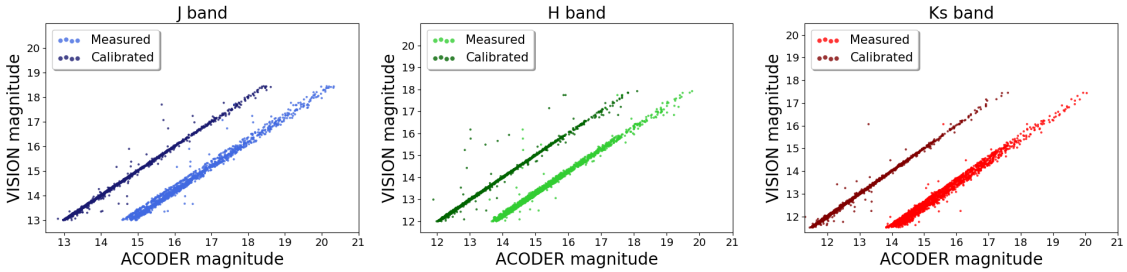

(a) Photometric calibration J band. **(b)** Photometric calibration H band. **(c)** Photometric calibration Ks band.

Figure 3.6: ACODER magnitudes vs VISION magnitudes. Light colors: measured magnitudes, dark colors: calibrated magnitudes for J band (left), H band (middle), and Ks band (right).

Similar to the seeing maps described in Section 2.1.1, there are also aperture correction maps available for the VISION mosaic. The calibration of the photometric measurements by ACODER are therefore accomplished as follows: The aperture correction value for each detected source and each band is read out individually from the aperture correction maps. All detected sources are corrected using these values. The so corrected magnitudes of targets which are also part of the ITC are plotted against their VISION magnitudes (VISION itself was calibrated using 2MASS). A linear fit to their distribution gives the calibration function for all detected sources. All three bands show a very good correlation of the corrected measured magnitudes to the linear fit, with correlation coefficients of 0.992, 0.989, and 0.996 for J, H and Ks respectively. Figure 3.6 shows the results of the photometric calibration.

3.8 The ACODER Output catalog

The above described tasks of ACODER are designed to ensure maximum quality of the output catalog. Therefore, targets that do not fulfill the requirements of ACODER are rejected. The possible reasons for rejection are the following:

- Target offset: no detected source within a radius of 3 pixels around the original VISION coordinates of the target
- Number of PSF contributors: insufficient number ($\leq$ 10) of high quality PSF contributors
- Photometry: failure of photometric measurements on the target by the IRAF task *phot*.
- PSF fitting: failure of PSF fitting on detected sources by the IRAF task *allstar*

Table 3.2 lists the targets that were affected by these problems, for the different bands. While ACODER rejects 147, 115, and 88 targets in J, H and Ks band respectively, only 134 are affected in more than one band and only 14 targets are rejected in all three bands.

Table 3.2: Targets which are rejected by ACODER.

Issue	J-band	H-band	Ks-band
Target offset	136	53	17
Nr. of PSF contributors	8	42	51
Photometry	3	16	1
PSF fitting	0	4	19
all	147	115	88

ACODER, at its current stage of development, is carried out individually on the different bands. For this work, due to the large input data set, the raw output catalogs for J, H and Ks contain 5640, 7280, and 6841 sources respectively. Before applying the filter for false positives, (see Section 3.8.2), these catalogs need to be combined and cross-matched. For the purpose of finding reliable CCs, this step has to be completed with high accuracy. The astronomical "Tool for OPerations on Calogues And Tables", TOPCAT (Taylor, 2005) was particularly designed for the efficient handling of such use cases. Therefore, even though it breaks the continuity of the automated routine, it is the most efficient and reliable method to accomplish this task. For the cross-match, a

maximum offset of 1 pixel in x and 1 pixel in y direction was allowed, even though at later stages, for the identification of false positives, partly different maximum errors were introduced (see Section 3.8.2). The resulting combined table contains 11,767 sources and is extended, where applicable, by the mean pixel, and sky coordinates, the mean distance to the primary, the calibrated photometry, and the 4th nearest neighbour (4NN) distance (see Section 3.10).

3.8.1 Duplicates

While combining the output tables it became clear, that some of the target sources are CCs to other target sources by themselves. Keeping this sources in the catalog for later analysis would, among other problems, lead to an overestimation of the CF, especially in regions with higher stellar density. To avoid this, the sources were internally cross-matched to the target sources in the combined ACODER output. All targets which match to a CC of another target, to which the CC has a separation of $\leqslant$ 15 pixels (r_{th}, see Section 3.9) are removed from the table. The true primary is identified by its brightness. In case there is a conflict between different bands, the longer wavelength band was given priority.

3.8.2 Identification of false positives

The main method for identifying reliable companion candidates as opposed to false positives was extensive testing on the training sample (described in Section 2.2.3). The final set of quality criteria for CCs was designed such, that the number of detected false positives towards the single sources in the training sample are is as low as possible, while the number of detected companions stays as large as possible. Based on the results of various test runs on the training sample, ACODER assigns a quality grade to each source, which is the result of a combination of various measurements. The following results lead to a bad quality grade: The failure of the PyRAF task imexamine in any of its measurements, values for the FWHM measurements of imexamine 5 pixels, FWHM values (derived from the R script) above 3 or below 2 pixels, a magnitude difference to the primary of more than 4 mag within a separation of 2 pixels (211 AU). Depending on the method used to detect the sources (directly or after subtraction), different grades are given for these problems. Finally, the grades are combined for all 3 bands and compared to the coordinate offsets of detections in different bands, or the lack of detections in more than one band, to yield a final quality grade. The capabilities of the so developed

selection criteria are further discussed and quantified in Section 4.2 and Section 4.3.2. Possible future refinements of this method are discussed in Section 6.

3.8.3 Visual examination with quick-DS9

As a last quality check, I manually searched for remaining false positives among all CCs within 15 pixels (r_{th}, see Section 3.9) that have passed the quality checks by the routine. In order to be able to decide whether or not a detected source is a proper star, or just a PSF feature, remnant from an incomplete subtraction, nebulosity, or outflow, all available data has to be compared at once. This includes the original, subtracted and second time subtracted image for all three bands, the coordinates of the detected sources and their quality marks.

The number of images generated in this work, however, is much too high to manually load image after image and search for all their corresponding processed images and the coordinates of all detected sources. To solve this problem and greatly speed up the examination process, I developed the quick-DS9 python routine. Quick-DS9 loads the set of three images (original, subtracted and second time subtracted), for all three bands into 3 $\times$ 3 frames into the SAOimageDS9 (Joye and Mandel, 2003) viewer, zooms in on the target, and marks the coordinates of all detected CCs and the target. By pressing one single button, the following, or previous set of images in the input ID-list is shown in the same way, or one can simply input a certain ID to see all the results. In addition, with a few clicks, quick-DS9 generates surface plots of regions of interest in a very simple manner, which makes it easy to compare e.g. PSF shapes to the images. This is especially important for the identification of nebulous features and outflows. False positives discovered during the visual examination are removed from the ACODER output table. The visual examination of the remaining detections would have exceeded the scope of this work. Thus, potential false positives with separations larger than 15 pixels ($\sim$ 5 arcsec) are not removed. The implications of potentially remaining false positives and the results of the visual examination are discussed in Section 4.3.2.

3.9 The statistical amount of bona fide companions

As mentioned in the beginning of this chapter, the VISION image data does not provide any information on stellar orbits. As a consequence, the actual multiplicity status of one single system cannot be determined with the method used in this work. Apparent binary systems could be pure line of sight coincidences. However, it was shown by e.g. Larson

(1995), that the separation distribution of the surface density of a certain stellar group reveals a regime of intrinsic multiple formation. This makes it possible to measure the total amount of bona fide companions towards a certain sample by using a statistical approach.

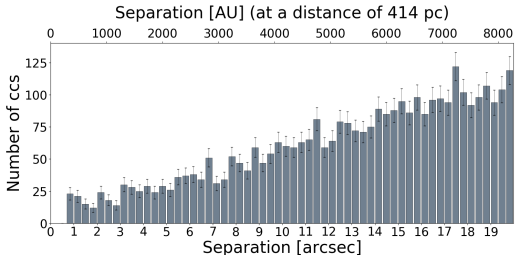

(a) Separation distribution of CCs towards the total sample.

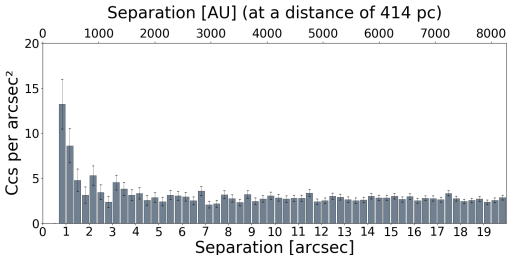

(b) Separation distribution of CCs per square arcsec towards the total sample.

Figure 3.7: Separation distributions of CCs towards the total target sample in bins of 0.333 arcsec. The black error bars show the errors on the number of companion candidates (CCs), calculated by using $\sqrt{n_{ccs(tot)}}$ where $n_{ccs(tot)}$ is the total number of detected CCs. Left: absolute number of detected CCs. Right: Number of CCs per square arcsec.

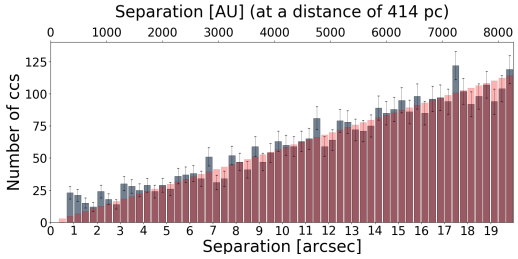

(a) Total number of CCs with background contamination in red.

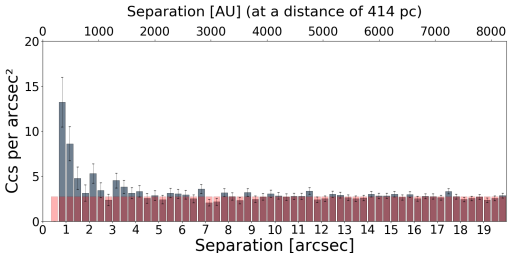

(b) Total number of CCs per unit area with background contamination in red.

Figure 3.8: Separation distributions of companion candidates (CCs) towards the total target sample in bins of 0.333 arcsec. The black error bars show the errors on the number of companion candidates (CCs), calculated by using $\sqrt{n_{ccs(tot)}}$, where $n_{ccs(tot)}$ is the total number of detected CCs. Red bars: estimated number of line of sight contaminants for each bin. For the contamination, the error is not shown here, because it is as small as ~ 0.05 for the total sample. Left: absolute number of detected CCs. Right: Number of CCs per square arcsec.

This method can be easily understood when taking a look at the separation distribution of all CCs. Figure 3.7a shows the total number of CCs towards the whole target sample, plotted against their separations to their corresponding primaries in bins of 0.333 arcsec (corresponding to 1 pixel). At this stage of the analysis, primaries are simply the targets found by the method described in Section 3.3. Physically, these sources could in fact themselves be companions to brighter stars as discussed in Section 4.3.

The increase of CC numbers towards the widest separations is a consequence of the increasing area covered by annuli with increasing radius. This fact is better understood when taking a look at the sketch shown in Figure 3.9.

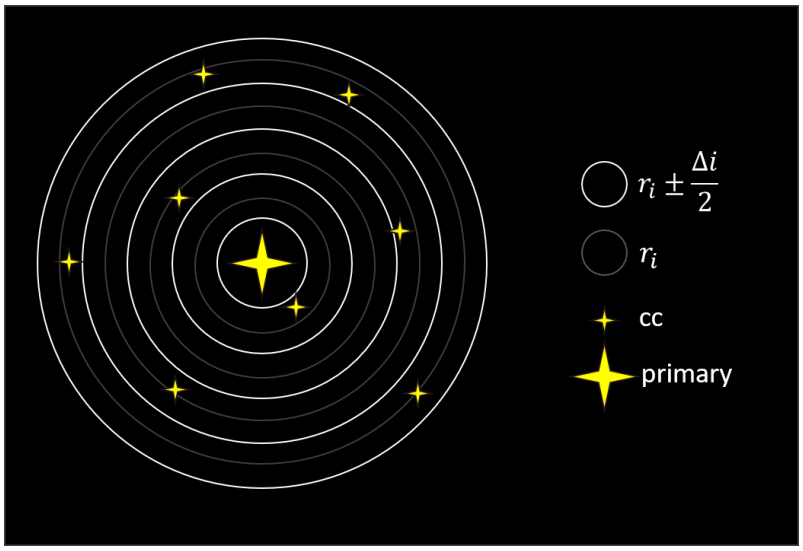

Figure 3.9: Sketch: With larger separations, the area covered by an annulus with radius r_i and width Δ_i increases correspondingly. If the surface density of background stars is constant, the average number of detected companion candidates (CCs) is a linear function of $2\Delta^2\pi i$.

Assuming a constant surface density of background stars, the number of CCs should be a linear function of the area. This becomes even more obvious when looking at the number of CCs per square arcsec, as shown in Figure 3.7b. The number of CCs per area is constant towards large separations, and the average number of line of sight contaminants per square arcsec ($\overline{n}_{cont}$) corresponds to the median CC number per square arcsec over all separation bins. However, there is an excess amount of CCs, towards smaller separations. The physical interpretation of this excess is, that it shows the number of actual, bona fide companions in the sample. By overplotting $\overline{n}_{cont}$ over each bin (Figure 3.8b), the threshold separation of bona fide companions (r_{th}), at ~ 5 arcsec becomes visible.

The total number of contaminants within r_{th} ($n_{cont(th)}$) is then calculated as follows:

$$n_{cont(th)} = \overline{n}_{cont} \cdot (r_{th}^2 \cdot \pi - r_0^2 \cdot \pi) \tag{3.1}$$

where r_0 is the separation below which the resolution is it not sufficient to detect any CCs.

The total number of bona fide companions (n_{comp}) in the sample is correspondingly calculated as follows:

$$n_{comp} = n_{ccs(th)} - n_{cont(th)} \tag{3.2}$$

where $n_{ccs(th)}$ is the sum of all detected CCs within 5 arcsec (r_{th}).

While $\overline{n}_{cont}$ can and should (due to potentially varying levels of extinction) be calculated individually for different sub-samples, the situation is different for r_{th}, as discussed in Section 4.3.3, Therefore, for this work, r_{th} is assumed to be 5 arcsec for all sub-samples. without this information.

3.10 YSO surface densities

For the aim of this work, a comparison of multiplicity properties between samples of YSOs in different environments (YSO surface densities) is obligatory. As a first attempt to do so, the YSO sample can be divided into a head and a tail sub-sample, motivated by the findings of Großschedl et al. (2018a) and Meingast et al. (2018) (see also Section 1.3).

Whereas this approach already reveals interesting results (see Section 4.1), a more physically motivated sample division is needed. To achieve this, the 4th nearest neighbor (4NN) distance for each YSO was calculated, using the haversine function. In order to make sure, that the apparent neighbors are all indeed part of Orion A and not simply background contaminants, only YSOs from the ITC were used for this calculation. Further, the Class III sources were excluded from the nearest neighbor analysis. Due to the limited field observed by Pillitteri et al. (2013), they are not evenly distributed across the VISION field and might therefore introduce a bias, if included in this part of the analysis. Figure 3.10 shows the 4NN distances of all YSOs (excluding Class III sources) in the ITC, and their positions in the sky.

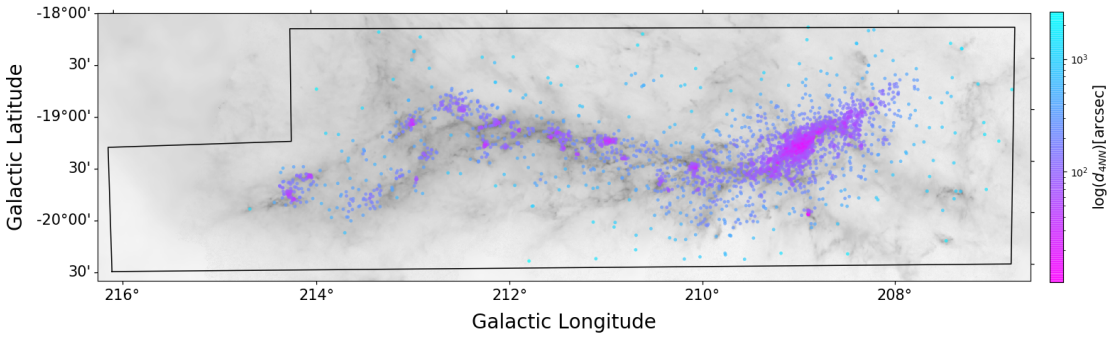

Figure 3.10: 4NN distances color-coded, for all YSOs in the ITC, except Class III sources distribution all YSOs in the ITC. Gray shaded background: Planck-Herschel-Extinction dust column-density map (Lombardi et al., 2014).

Chapter 4

Results and Discussion

4.1 Companion fractions in Orion A

For all targets for which ACODER was successfully executed, the available information about the target (primary) itself, its companion candidates (CCs) and the multiplicity status of the system are combined. The resulting multiplicity catalog for Orion A will hereafter be called MCO. This catalog is used to calculate the number of bona fide companions (n_{comp}) with the method described in Section 3.9 and subsequently the companion fraction (CF). As explained in Section 1.4, the CF, gives the average amount of companions for each primary in a certain target and should not be confused with the multiplicity fraction (MF). The CF is calculated as follows:

$$CF = \frac{n_{comp}}{n_{prim}}, \tag{4.1}$$

where n_{prim} is the number of target YSOs, that were selected as described in Section 3.3. As noted already in Section 3.9, these target YSOs could in fact themselves be CCs to even brighter stars. This issue is discussed in Section 4.3. The errors of the CF values are calculated, following the standard method of error propagation and assuming that the error on the sample size (n_{prim}) is poisson distributed.

$$CF \cdot \frac{1}{\sqrt{n_{prim}}} \tag{4.2}$$

This assumption might lead to an underestimation of the actual error, since it does not account for any systematic error sources. A potential improvement of the error estimation is presented in Section 6.1 and the potential effects of known additional

uncertainties are discussed in Section 4.3

In order to investigate the dependencies of stellar multiplicity on evolutionary stage and environmental properties, different sub-samples of YSOs were taken for comparison. As mentioned in the very beginning of this work, in Section 1.3, Orion A hosts regions with distinct properties, such as stellar surface densities. Therefore, based on recent work by Großschedl et al. (2018b), who find that Orion A tilts backwards, away from the observer at a Galactic Longitude of around 210°, the sample is divided into an eastern (E) and a western (W) sample, which they also call the "Head" and the "Tail" of Orion A. While this division already leads to interesting results, a more physically motivated sub-division into samples with different YSO surface densities is needed. Using the 4NN distances described in Section 3.10, the sample was divided into a high-density (H) sample (4NN distances $\leq$ 130 arcsec), and a low-density (L) sample (4NN distances 130 arcsec). The threshold values for the 4NN distances are chosen such, that the sample sizes of both samples remain comparable. The sample which contains all YSOs from all regions and all densities is called the total sample (T). The number of CCs, the contamination fraction, as well as the CF are separately estimated for the different samples and discussed in this section.

Table 4.1: Results for the total sample.

sample	CF	n_{prim}	$n_{ccs(th)}$	$n_{cont(th)}$	n_{comp}	q_{cont}
P	12.22 $\pm$ 1.31 %	87	16	5.36	10.64	33.51 %
F	9.37 $\pm$ 0.89 %	110	19	8.69	10.31	45.74 %
D	3.50 $\pm$ 0.09 %	1368	239	191.08	47.92	79.95 %
III	4.22 $\pm$ 0.26 %	270	44	32.61	11.39	74.12 %
T	4.16 $\pm$ 0.10 %	1835	318	241.71	76.29	76.01 %

Figure 4.1 and Table 4.1 show the results for different evolutionary stages of YSOs in the total sample (P, F, D, III). Figure 4.2, Table 4.2, and Table 4.3 show the results for different regions of Orion A (E, W). Figure 4.3, Table 4.4, and Table 4.5 show the results for different YSO surface densities (L, H). The tables shown in this section give the number of target sources (n_{prim}), the number of CCs within r_{th} ($n_{ccs(th)}$), the number of contaminants within r_{th} ($n_{cont(th)}$), the number of bona fide companions (n_{comp}), and the contamination fraction (q_{cont}) which is calculated as follows:

$$q_{cont} = \frac{n_{cont(th)}}{n_{ccs(th)}}. \tag{4.3}$$

For all listed sub-samples, the P refers to protostars, the F to flat spectrum sources,

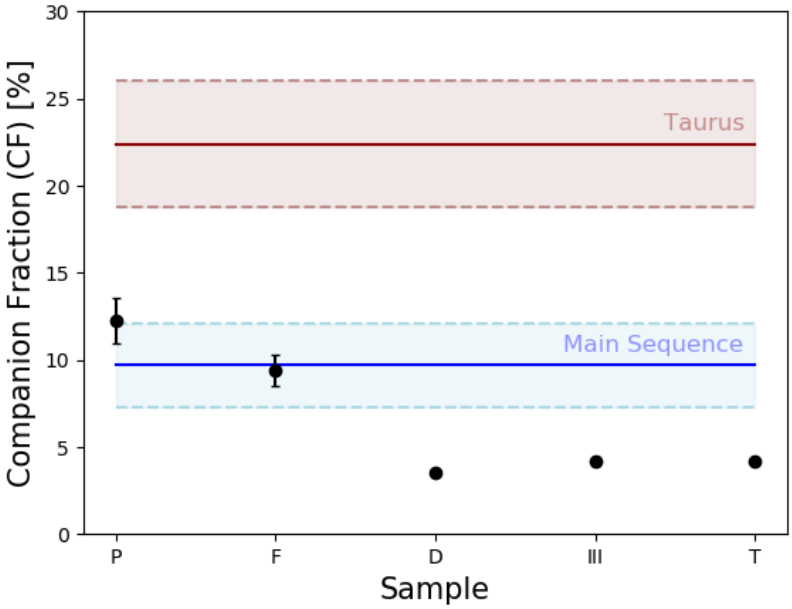

Figure 4.1: CF of different YSO classes, for the total sample. Red line and red shaded region: Estimated value for Taurus (Leinert et al., 1993; Kohler and Leinert, 1998) ± errors, blue line and blue shaded region: estimated value for the Main Sequence (Duquennoy and Mayor, 1991) ± errors. Black dots (from left to right) CF values for: protostars (P), flat spectrum sources (F), pre-main sequence stars with disks (D), Class III sources (III) and the total sample (T), with errors. For the three latter samples, the errors are too small to be visible on this plot.

the D to disks, and the III to Class III sources within the sample. The single letter (T, E, W, L, H) refers to the combined value of the whole sample. The CF values for Taurus (in red) and the MS (in blue), that are shown in the figures in this section are calculated for the separation range of this study and provided by Rainer Köhler (personal communication), who used the results of Leinert et al. (1993); Kohler and Leinert (1998) for Taurus and Duquennoy and Mayor (1991) for the MS.

Table 4.2: Results for the eastern sample (E).

sample	CF	n_{prim}	$n_{ccs(th)}$	$n_{cont(th)}$	n_{comp}	q_{cont}
EP	15.96 ± 1.95 %	67	15	4.31	10.69	28.72 %
EF	11.06 ± 1.29 %	73	14	5.93	8.07	42.35 %
ED	5.53 ± 0.24 %	554	99	68.34	30.66	69.03 %
EIII	5.58 ± 0.45 %	152	25	16.53	8.48	66.10 %
E	7.25 ± 0.28 %	694	128	77.71	50.288	60.72 %

Towards the 1835 stars in the main sample, I find 318 companion candidates (CCs)

Table 4.3: Results for the western sample (W).

sample	CF	n_{prim}	$n_{ccs(th)}$	$n_{cont(th)}$	n_{comp}	q_{cont}
WP	5.00 ± 1.12 %	20	1	0.00	1.00	0.00 %
WF	3.92 ± 1.45 %	37	5	3.55	1.45	70.99 %
WD	2.31 ± 0.08 %	814	140	121.22	18.78	86.58 %
WIII	5.01 ± 0.46 %	118	19	13.09	5.91	68.90 %
W	2.03 ± 0.07 %	871	146	128.29	17.71	87.87 %

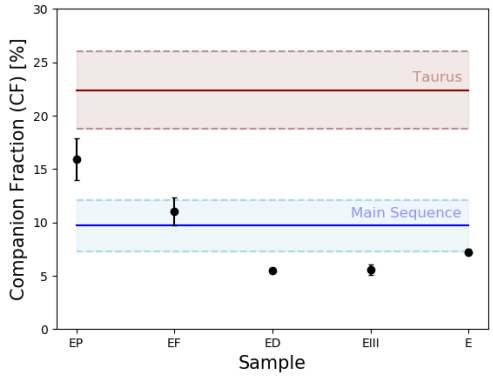

(a) CF values for eastern sample (E).

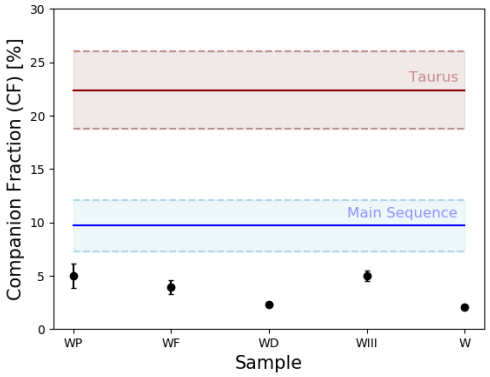

(b) CF values for western sample (W).

Figure 4.2: CF values for the different YSO classes in the eastern sample (left) and the western sample (right). Least evolved YSOs are on the leftmost side (P), more evolved sources to the right. The rightmost sample gives the value for the whole sub-sample. Red line and red shaded region: estimated value for Taurus (Leinert et al., 1993; Kohler and Leinert, 1998) ± errors, blue line and blue shaded region: estimated value for the Main Sequence (Duquennoy and Mayor, 1991) ± errors.

within 5 arcsec (r_{th}) of their primary. I estimate, that 76.01 % of these are caused by line of sight coincidences, which leaves a total CF of 4.16 ± 0.10 %.

The overall CF for the total sample is with 4.157 % lower than expected, when compared to the values for Taurus (e.g. Leinert et al., 1993; Kohler and Leinert, 1998) and the Main Sequence (Duquennoy and Mayor, 1991). This might be due to the fact, that, at its current state, ACODER overestimates the number of contaminants, leading to an overall lower result for the CFs of all samples. However, correcting for this issue would very likely even enhance the qualitative results of this work, as discussed in more detail in Section 4.3.

It should be mentioned here, that the resulting value for the CF of the total sample is not the same as the weighted average for all sub-samples, since the contamination fraction is estimated separately for each sample, as described in Section 3.9.

The results of the CF values for different samples are the following: All samples show

Table 4.4: Results for the low-density sample (L).

sample	CF	n_{prim}	$n_{ccs(th)}$	$n_{cont(th)}$	n_{comp}	q_{cont}
LP	16.61 ± 2.60 %	41	9	2.19	6.81	24.35 %
LF	8.23 ± 1.29 %	41	8	4.62	3.38	57.80 %
LD	1.43 ± 0.05 %	503	125	114.95	10.05	91.96 %
L	2.58 ± 0.09 %	785	142	121.75	20.25	85.74 %

Table 4.5: Results for the high-density sample (H).

sample	CF	n_{prim}	$n_{ccs(th)}$	$n_{cont(th)}$	n_{comp}	q_{cont}
HP	9.68 ± 1.43 %	46	7	2.55	4.45	36.36 %
HF	9.70 ± 1.17 %	69	11	4.31	6.69	39.16 %
HD	5.83 ± 0.23 %	665	114	75.22	38.78	65.96 %
H	6.38 ± 0.23 %	780	132	82.23	49.77	62.30 %

a decrease of CF values from the youngest YSOs (P), to the more evolved sources (D). This decrease is most prominent in the low-density sample, where the CF decreases from 16.6 % to 1.43 % from P to D, and in the eastern sample, where it decreases from $\sim$ 15.96 % to 5.53 % from P to D. For the high-density, and the western sample, the CF difference between the P and F sample seems to be insignificant within the errors, while there is a again a decrease towards the D sample. The CF drops from 9.68 % to 5.83 % for the high-density sample and from 5 % to 2.31 % for the western sample, from P to D. The Class III sources in the western sample do not follow this trend, and have a higher CF value of 5.01 %, similar to the protostars in this sample. While this is surprising and definitely needs further investigation (see Section 6), the Class III sources close to the ONC are though to likely be foreground sources. If true, the study conducted with ACODER probes a much broader separation range for these sources than for the other YSOs, because much closer companions can be resolved if the distance to this sources is lower. On the other hand, the CF of the Class III sources in the eastern sample is consistent of the one obtained for the disks. In general, the results for Class III sources have to be considered more carefully, since these are the most evolved and at least some of them will certainly have already moved farther away from the cloud. One of the most surprising results is the difference in total CF for the high-density and the low-density samples. While the combined result for the low-density sample is a relatively low CF of 2.58 %, the combined CF of the high-density sample is with 6.38 % 2.5 times higher. This apparent dependency of CF on YSO surface density is however mostly dominated by the disk sources, since they are the most numerous. On the other hand, the values for

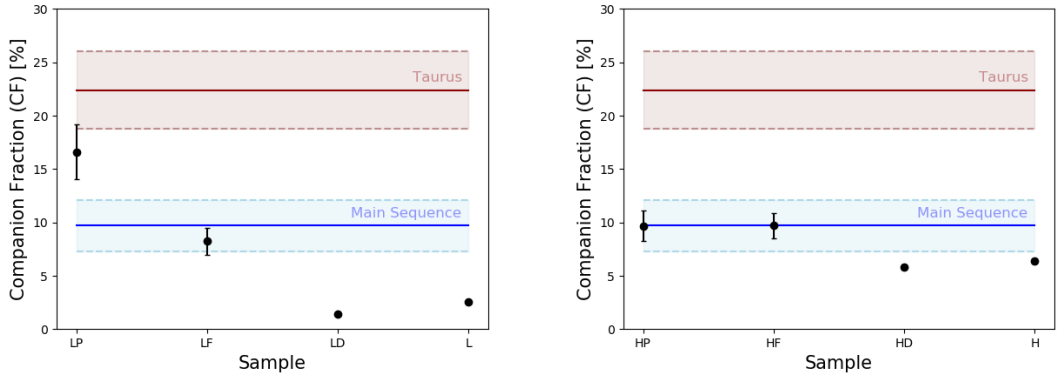

(a) CF values for low-density sample (L). **(b)** CF values for high-density sample (H).

Figure 4.3: CF values for different YSO classes in the low-density sample (left, 4NN $\leq$ 130 arcsec) and the high-density sample (right, 4NN 130 arcsec). of different YSO surface densities. Red line and red shaded region: Estimated value for Taurus (Leinert et al., 1993; Kohler and Leinert, 1998) $\pm$ errors, blue line and blue shaded region: estimated value for the Main Sequence (Duquennoy and Mayor, 1991) $\pm$ errors.

the flat spectrum sources are equal in the high and low-density sample. In general, I do find a significant decrease in CF towards more evolved YSOs in the total, the Tail and the loose sample, while the CFs of the other samples seem to be almost independent of evolutionary stage.

This findings appear to suggest multiple conclusions:
First, the number of multiple systems within a certain sample decreases independently of stellar encounters in dense systems. If this was not the case, the CFs in the loose and the Tail sample would remain constantly high over all evolutionary stages. This suggests, that the disruption of multiple systems is therefore likely an intrinsic process, stemming from the decay of higher order multiples, where one component gets ejected while the closer component moves further inward, and becomes undetectable for studies like this one. Kounkel et al. (2016) on the other hand do not find such an evidence for intrinsic decay of multiple systems. There are various potential reasons for this, but the main reason for concern towards the analysis by Kounkel et al. (2016) is their relatively low number counts, which simply might not allow for a further sub-division into multiple samples. The inclusion of even more YSOs in future studies with ACODER will certainly help to further constrain the true nature of the results shown in this work.

Second, the CFs seem to stay much more constant with evolutionary stage within the high-density and the western sample. Combined with the result for the other samples, this seems to suggest, that for the high-density, and the western sample, the intrinsic

decay is terminated earlier and equilibrium is reached sooner. Correspondingly the decay of multiple systems, from protostars to more evolved YSOs can not be observed to such an extent as it is the case for the remaining samples.
Third and less straight forward, the number for the total CF, found for the high-density sample is higher than the one for the low-density sample. This seems to suggest, that while the decay of multiple systems in dense regions is terminated earlier, CF numbers overall remain higher. Kounkel et al. (2016) find a similar trend in their study. They state, that this might indeed suggest, that the denser regions of Orion A (not including the ONC) primordially produce more stellar multiples.

One possible way of improving our understanding of these results on young multiples, is a further subdivision into Class 0 and I sources and more different density samples. For this, it is crucial to include as many of the previously excluded sources as possible, in order to increase the sample sizes.

Overall, the CF values found in this work are relatively low. One reason for this might be the very strict ACODER approach, that was necessary to guarantee the exclusion of the majority of false positives without a the need of a visual examination of each image. On the other hand some potentially remaining false positives at high separations and the subsequent overestimation of the contamination fraction, as well as incompleteness also contribute to the low numbers obtained in this work. The quantitative results of this work should therefore be considered as a lower limit to the actual values. Future refinements of the method will very likely lead to a larger number of detected companion candidates.

4.2 Completeness

With an average seeing of $\sim$ 0.8 arcsec, VISTA's theoretical resolution limit, in terms of physical separation at a distance of 414 pc, (Menten et al., 2007) is roughly 330 AU. Even binaries at much smaller separations are revealed by ACODER, if the magnitude difference between the two stars is small. As an example, Figure 4.4a shows the VISION image of the binary system HOPS 286, with an estimated separation of only 96 AU and a Δm of $\sim$ 0.6 mag in H band (Kounkel et al., 2016). The subtraction of a single star PSF (Figure 4.4b) in the center of this source leaves two residuals, indicating, that the source is in fact a binary system. A comparison with the binary components' positions found by Kounkel et al. (2016), reveals a perfect match with the two residuals, with respect to position angle. In this manner, almost all binaries in the training sample, with separations down to 96 AU can be identified by visual examination. Unfortunately,

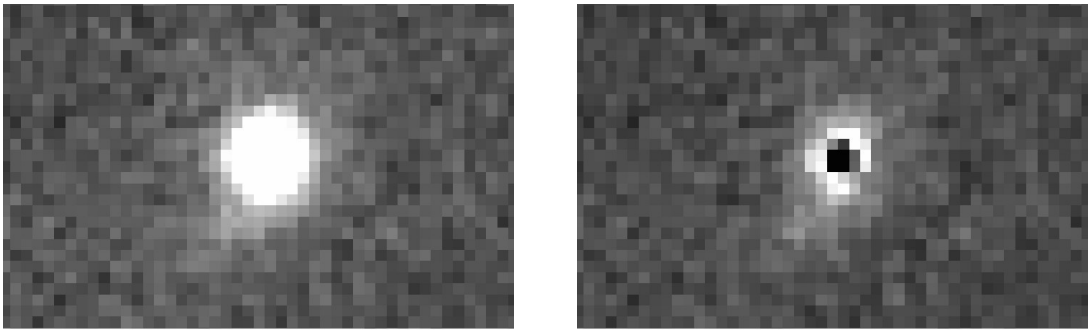

(a) Binary system HOPS268 before subtraction. **(b)** Binary system HOPS268 after subtraction.

Figure 4.4: The binary system HOPS286, with an estimated separation of only 96 AU and a ΔM of $\sim$ 0.6 in H band (Kounkel et al. (2016)), before (a) and after subtraction (b). The subtraction of a single star PSF in the center of this source leaves two symmetrical residuals, indicating, that the source is in fact not single.

all attempts for an automated detection, photometric measurements or even the proper estimation of the separation, fail in such cases, because the residuals cannot be properly fit. At the current stage of development of ACODER, such sources therefore have to be considered as missed.

With the available training sample, which was observed with much better resolution, it is possible to roughly determine the limits of ACODER in terms of separation and magnitude difference (ΔM). Of the binary systems studied by Kounkel et al. (2016), 35 are also found in the VISION catalog. Among these, 26 were not affected by the problems described in Section 2.2.2, and were successfully processed with ACODER. With the developed detection routine, 50 % of all companions to these 26 stars were successfully recovered with ACODER, confirmed by visual examination and photometric measurements could be carried out on them. Using the separation values and magnitudes found in Kounkel et al. (2016) a first and rough completeness estimate could be carried out, by comparing the properties of the detected companions to the missed ones. The magnitude differences given here, are only rough estimates of the actual values, since in most cases, measurements are available only for one band in Kounkel et al. (2016). If possible, the values were taken from their WF160W or NF160W band which corresponds to the H band and otherwise from their NF205W band. Using the magnitudes estimated on the VISTA images at the current stage is not useful, since they cannot account for the missed companions and still have to be calibrated. Figure 4.5 shows the separations and magnitude differences of the 13 missed companions (red) and the 13 recovered ones (blue), to their primaries.

The closest separation among the successfully detected binary systems, is 229 AU

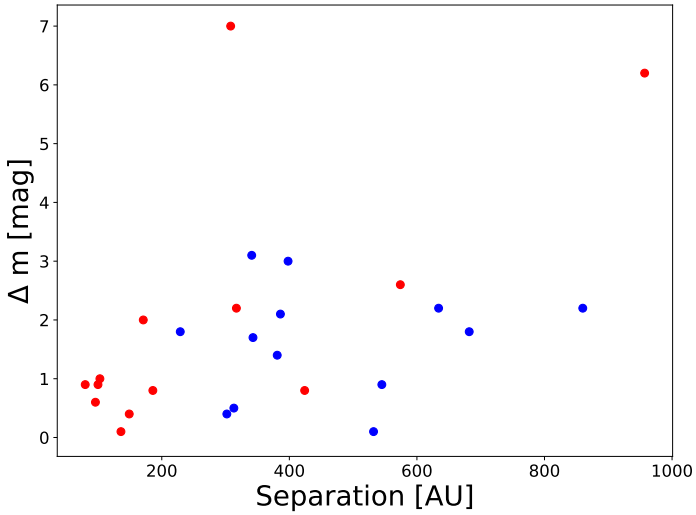

Figure 4.5: Separations and magnitude differences of the subset of the 26 binary systems in the training sample. Red: 13 companions missed by the detection routine. Blue: 13 companions detected by the routine.

with a magnitude difference of 1.8 mag, while the largest magnitude difference is 3.1 mag at a separation of 341 AU. In cases where companions with a separation well above 300 AU have not been detected, the companions are very faint with H-band magnitudes $>$ 19.6 and fall even below a detection threshold of 5 σ, although in three cases, they are clearly visible on the subtracted images. Some further refinements of the routine might help to even recover these very faint sources. Giving a completeness estimate is difficult, since the training sample is small. At the current state, it can only be noted, that all companions with separations $\geq$ 229 AU, Δ m $\leq$ 2 and M_H $<$ 19.6 of the targets in the training sample that are not either saturated or to faint, are successfully recovered.

4.3 Caveats of ACODER

4.3.1 Identification of primaries

As mentioned in Section 3.9, identifying the primary of a multiple system is not completely straight forward. Due to the exclusion of some target YSOs (see Section 2.2.2), some of the so-called primaries in the MCO could in fact be CCs to such YSOs that were removed before. However, in order to reduce the risk of detecting false positives, targets YSOs with a separation $\leq r_{th}$ to a neighboring target YSO that is flagged as saturated,

have been removed from the MCO. Also, target YSOs which match to a CC-detection of another, brighter target YSO have been removed from the MCO, as described in Section 3.8. This certainly leads to a loss of CCs, due to the fact that some of the removed CCs might not have been detected on the image of the respective neighboring, brighter YSO, or might have separations r_{th} towards the brighter YSO. The inclusion of the CCs that are potentially lost in this step is therefore one of the priorities of future refinements of ACODER.

4.3.2 Remaining false positives

In the training sample of known single stars, 160 do not suffer from the problems described in Section 2.2.2 and are successfully processed with ACODER. Almost all faulty detections, closer than 5 arcsec (r_{th}) to one of the single sources in the training sample were successfully identified by applying the restrictions described in section 3.8.2. On the other hand, 7 of them remained unaccounted for. These $\sim$ 4 % of false positives would make $\sim$ 81 for the whole sample of 1835 YSOs in the MCO. Indeed, after the visual examination (Section 3.8.3), 79 false positives with separations $\leq r_{rh}$ were detected and removed. Unfortunately, potential false positives with larger separations were not removed, since the time demand of this procedure would not have been feasible within the scope of this work. Overall, these remaining false positives therefore lead to an overestimation of $\overline{n}_{cont}$ and a subsequent underestimation of the CF. The distribution of the already excluded false positives showed, that they are almost three times as numerous (58 vs. 21) in the eastern part of Orion A. The reason for this is very likely the available number of suitable PSF contributors, which is naturally lower in large regions with low surface density. Hence, a correction for these potential false positives would most likely lead to an enhancement of the the differences between the eastern and western sample. One might conclude, that the difference in the distribution of false positives is the same for the low and high-density sample. This is however not the case. The number of excluded false positives in the low-density sample is only 1.4 times higher than the one in the high-density sample (46 vs 33). Even though a correction for false positives with large separations would bring the CF numbers for these two samples closer together, it can still not account for the large difference between them. The general qualitative result would therefore very probably not change after a correction for potential remaining false positives. In order to gain additional confidence concerning the quantitative results, such a correction should definitely be part of future refinements of ACODER. One possibility to avoid this problem at all, would be to use only sources from the VISION catalog for

separations larger than r_{th}.
While this approach might decrease the number of false positives, (although the VISION catalog itself is also not free of false positives) it has some disadvantages to it. The most obvious is that the detection limits, chosen for the compilation of the VISION catalog are not the same as of ACODER. In ACODER, due to the sophisticated identification system, even very faint sources were successfully identified as CCs. The source extraction methods used for the VISION catalog and the MCO are in general different. Matching the two catalogs would therefore require thorough adjustments, which again could lead to a reduction of the number of bona fide companions in the MCO.
On the other hand, future refinements of ACODER (see Section 6) will hopefully make the effort of combining the MCO with the VISION catalog superfluous and generally lead to a decrease of false positives.

4.3.3 Non-uniformity of input data

Großschedl et al. (2018a) show that the assumed distance of 414 pc towards the whole Orion A cloud (taken from Menten et al., 2007) is not correct. In fact, Orion A seems to bend backwards, east of a galactic longitude of 210°. While their estimated YSO distances in the head of Orion A are on average 390 to 395 pc, the ones in the tail lie between $\sim$ 400 and $\sim$ 470 The number of resolved CCs, towards small separations is therefore smaller in the Tail, than in the Head. The number of contaminants is overestimated for all samples, due to incompleteness towards the smallest resolved separations. Due to the farther distance of (at least part of) the Tail this effect is even stronger for the Tail. A fair comparison between the resulting CF of the Head and the Tail would therefore have to apply the same incompleteness cuts to the CCs found in the Head. Correcting for the distance gradient would therefore lead to an enhancement of the CF differences between the Tail and the Head. With the currently available data e.g. from Gaia, this is however not possible. Großschedl et al. (2018a) only find distances for a part of the YSOs in Orion A. While this helps Großschedl et al. (2018a) to estimate the average distance to the cloud, the scatter in YSO distances would make a distance correction for the estimated CF values very complicated and prone to errors.
Another issue that should be mentioned is, that due to different stellar densities, the threshold separation for bona fide companions (r_{th}) could vary among different samples. However, due to the much lower sample sizes of some samples, an estimation of r_{th}, using only the sub-sample is much more error prone, than when using the total sample. Therefore the value of 5 arcsec is consistently used for all samples.

Chapter 5

Conclusions

The main goal of this work is to investigate the multiplicity properties towards the largest known sample of young visual binaries towards one single star-forming region with an Automated Companion DEtection Routine (ACODER). ACODER is a python/PyRAF routine, that automatically accomplishes source detection, PSF fitting, and subtraction, as well as quality flagging on VISTA NIR images. The initial target catalog for this work contains 3386 Young Stellar Objects (YSOs), located in Orion A, taken from Großschedl et al. (2018b) and Pillitteri et al. (2013). Due to saturation, overcrowding, and other reasons (described in Section 2.2.2), in this work, only part of the sample was analyzed with ACODER. Including the remaining sources in the analysis is the subject of future work. The final multiplicity catalog for Orion A (MCO) contains 1835 primary YSOs, for which 318 companion candidates (CCs) were found within the threshold separation of 5 arcsec (r_{th}). A statistical analysis of the separation distribution shows that 241.71 of these CCs are line-of-sight contaminants. This estimates to 76.29 bona fide companions and a companion fraction of 4.16 $\pm$ 0.10 % for the total sample. Overall this value is lower than what is found by e.g. Leinert et al. (1993) or Kohler and Leinert (1998). The most significant result of this study is the finding of a clear age-dependent CF in all samples. While the estimated CF for the protostars is highest (12.22 $\pm$ 1.31 % for total sample), it is lowest for the more evolved pre-main-sequence stars with disks (3.50 $\pm$ 0.09 %). This finding, in combination with previous findings of other studies of pre-main-sequence stellar multiplicity, strongly suggests a decay of wide multiple systems with age, regardless of the environment.

For the eastern and the western sample, I find a quite remarkable difference in CF numbers, with a CF of 7.25 $\pm$ 0.28 % in the eastern, and 2.03 $\pm$ 0.07 % in the western sample. This finding shows once again, that Orion A hosts two very distinct

star formation sites, as found already by e.g. G18, Meingast et al. (2018). Surprisingly, when comparing the total sample with 4NN distances $\leq$ 130 arcsec, and 4NN distances 130 arcsec, for which I estimate a CF of 6.38 $\pm$ 0.23 % and 2.58 $\pm$ 0.09% respectively, this trend seems to be reversed. When taking a closer look at the CF values for the different sub-samples, however, one trend seems to be equal for the low-density and the eastern sample. In both these samples, the Protostar sub-sample (LP, EP) shows a much higher CF value than in the corresponding counterpart of the high-density and the western sample (HP, WP).

Although ACODER, at the current stage of development, leads to an underestimation of the number of CFs, the results and low statistical errors obtained in this work show that ACODER is a powerful tool for obtaining statistically significant information about the multiplicity properties in large data sets. While the study presented in this work is by not complete in terms of different environments or separation ranges, it levels the ground for a new generation of big data studies of stellar multiples in entire star-forming regions.

Chapter 6

Future work

6.1 Refining ACODER

For this work, the analysis and combination of CC parameters, such as photometry, position - offsets, and multiple detection was done manually by comparison with the training sample. This, however, is a typical use case for machine learning tools. Combining all measured parameters into a parameter hyperspace and automatically comparing them to the parameters of already verified multiple systems from this work, will certainly enhance the power of ACODER as an automated companion detection routine for future NIR surveys.

The main goal of ACODER is automating the companion detection towards large samples of YSOs. The most crucial step in the development of ACODER is the testing, so a well-defined training sample is therefore key for a successful companion detection. Also, for implementing machine learning in a future ACODER version, a well-defined training sample is needed. As described in Section 4.3.2, ACODER at its current stage of development can not account for all false positives. While it seems feasible to accomplish visual examinations for small sub-samples, e.g., with quick-Ds9 (3.8.3), this is not practical for large samples. Fortunately, there are various methods for future refinements of ACODER to exclude further constrain and remove false positives. First, the results of this work will serve as a starting ground for further testing. While for this work, only a small training sample of previously studied binaries and singles was available, the MCO produced in this work provides a much more extensive training sample for future studies. Second, a sample of well defined single stars with fake companions can lead, in addition, to useful constraints on the exclusion of false positives. Generating such a sample, however, can be challenging and demands a thorough analysis of the quality of

the inserted fake stars. Such analysis is beyond the scope of this work and the subject of future work. One of the main advantages of such a fake star analysis is that it can be used to constrain the completeness, the discovery space of separation and magnitude difference between primary and companion, as well as any potential systematic errors. A fake star analysis would help to correctly put the results of this work in a broader context.

Apart from the above mentioned possible future refinements of ACODER, further work could also include the testing of the following refinements: At its current stage, ACODER accounts for seeing variations across the VISION mosaic by cutting sub-images from the mosaic that correspond to one detector size of VISTA. This procedure does not account at the moment for possible edges of certain seeing conditions that might occur within this sub-image. Allowing ACODER to vary the size and shape of these sub-images, based on the seeing maps for VISION might be very beneficial for the subsequent PSF fitting procedure. Further, the number of well behaved PSF contributors is too low on some images, especially in regions with low stellar surface density. While it has proven crucial to restrict the allowed properties of these contributors, one possible solution to this problem could be the allowing of a larger sub-image for such cases. This, however, needs to be tested, as it could as well have a negative effect on the number of detected false positives.

6.2 Inclusion of problematic sources

As mentioned in Section 2.2.2, 1421 YSOs have been excluded from the analysis carried out in this work. For the 61 most severely affected sources, the ones that are saturated on the VISTA images, in all three bands, a follow-up observation was carried out using the NACO instrument of the VLT UT1. While the analysis of these new image material was not subject of this work, it will contribute to an even more complete multiplicity catalog of Orion A in the future. For a significant fraction of the less severely affected sources, however, an improved version of ACODER will undoubtedly lead to high-quality results as well. Including more YSOs close to the ONC will be particularly interesting for comparisons of the multiplicity properties of different sub-regions of Orion A. Some of the sources that have been excluded might actually be less problematic. The development of an additional tool that helps ACODER to identify such sources would, therefore, quickly lead to even better statistics and likely exciting information about the regime that is not probed in this work. In Section 3.8.1, the removal of sources which are themselves CCs to other targets is described. However, such sources could provide interesting information

on the clustering of multiple systems, as described, for example, in Joncour et al. (2018) for similar findings in Taurus. Future work on the sample of YSOs in Orion A should, therefore, emphasize also on the study of such systems.

6.3 Additional data

In order to correct for possible distance variations, both, across the whole cloud and among Class III sources, 3D positions should most definitely be added to the data set that was studied in this work. Even though most of the YSOs that were the subject of this work are not in the Gaia catalog, due to their maximum at long wavelengths, some are, as shown for example in Großschedl et al. (2018a). For these sources, their separations can be estimated more accurately. Obtaining 3D positions or proper motions for (some of) the detected CCs can help to further converge the multiplicity properties of the individual systems in Orion A and might reveal even more potentially useful information for further analysis. Newly available data from large NIR surveys, such as the VISTA star formation atlas, VISIONS[1], will additionally enhance the available data that can be used for studies of young multiples. Tools like ACODER are designed for the analysis of statistically significant samples of young multiples, in combination with newly available data, and have the potential to improve our understanding of the formation of stellar multiples, and therefore star formation in general. With upcoming technologies of even higher resolution, such studies might extend far beyond the solar neighborhood in the future and reveal the properties of binary formation in very different star-forming regions than the ones we know well so far. Almost certainly, with every new piece of the puzzle of understanding star formation, there will come a new unanswered question.

[1] https://www.eso.org/sci/observing/PublicSurveys/sciencePublicSurveys.html, https://visions.univie.ac.at

References

ALMA Partnership, C. L. Brogan, L. M. Pérez, T. R. Hunter, W. R. F. Dent, A. S. Hales, R. E. Hills, S. Corder, E. B. Fomalont, C. Vlahakis, Y. Asaki, D. Barkats, A. Hirota, J. A. Hodge, C. M. V. Impellizzeri, R. Kneissl, E. Liuzzo, R. Lucas, N. Marcelino, S. Matsushita, K. Nakanishi, N. Phillips, A. M. S. Richards, I. Toledo, R. Aladro, D. Broguiere, J. R. Cortes, P. C. Cortes, D. Espada, F. Galarza, D. Garcia-Appadoo, L. Guzman-Ramirez, E. M. Humphreys, T. Jung, S. Kameno, R. A. Laing, S. Leon, G. Marconi, A. Mignano, B. Nikolic, L. A. Nyman, M. Radiszcz, A. Remijan, J. A. Rodón, T. Sawada, S. Takahashi, R. P. J. Tilanus, B. Vila Vilaro, L. C. Watson, T. Wiklind, E. Akiyama, E. Chapillon, I. de Gregorio-Monsalvo, J. Di Francesco, F. Gueth, A. Kawamura, C. F. Lee, Q. Nguyen Luong, J. Mangum, V. Pietu, P. Sanhueza, K. Saigo, S. Takakuwa, C. Ubach, T. van Kempen, A. Wootten, A. Castro-Carrizo, H. Francke, J. Gallardo, J. Garcia, S. Gonzalez, T. Hill, T. Kaminski, Y. Kurono, H. Y. Liu, C. Lopez, F. Morales, K. Plarre, G. Schieven, L. Testi, L. Videla, E. Villard, P. Andreani, J. E. Hibbard, and K. Tatematsu. The 2014 ALMA Long Baseline Campaign: First Results from High Angular Resolution Observations toward the HL Tau Region. *ApJ*, 808(1):L3, July 2015. doi: 10.1088/2041-8205/808/1/L3.

J. Alves, C. Lada, and E. Lada. Seeing the light through the dark. *The Messenger*, 103:1, March 2001.

John Bally. Overview of the orion complex, 2008.

Bart J. Bok and Edith F. Reilly. Small Dark Nebulae. *ApJ*, 105:255, March 1947. doi: 10.1086/144901.

Alexis Brandeker, Ray Jayawardhana, Parandis Khavari, Jr. Haisch, Karl E., and Diego Mardones. Deficit of Wide Binaries in the η Chamaeleontis Young Cluster. *ApJ*, 652 (2):1572–1584, Dec 2006. doi: 10.1086/508483.

G. Duchêne and A. Kraus. Stellar Multiplicity. *ARA&A*, 51:269–310, August 2013. doi: 10.1146/annurev-astro-081710-102602.

G. Duchêne, S. Lacour, E. Moraux, S. Goodwin, and J. Bouvier. Is stellar multiplicity universal? Tight stellar binaries in the Orion nebula Cluster. *MNRAS*, 478(2): 1825–1836, August 2018. doi: 10.1093/mnras/sty1180.

A. Duquennoy and M. Mayor. Multiplicity among solar-type stars in the solar neighbourhood. II - Distribution of the orbital elements in an unbiased sample. *A&A*, 248:485–524, August 1991.

J. Emerson, A. McPherson, and W. Sutherland. Visible and Infrared Survey Telescope for Astronomy: Progress Report. *The Messenger*, 126:41–42, December 2006.

T. P. Greene, B. A. Wilking, P. Andre, E. T. Young, and C. J. Lada. Further mid-infrared study of the rho Ophiuchi cloud young stellar population: Luminosities and masses of pre-main-sequence stars. *ApJ*, 434:614–626, October 1994. doi: 10.1086/174763.

J. E. Großschedl, J. Alves, S. Meingast, and B. Hasenberger. 3D shape of Orion A with Gaia DR2. An informed view on Star Formation Rates and Efficiencies. *arXiv e-prints*, December 2018a.

J. E. Großschedl, J. Alves, P. S. Teixeira, H. Bouy, J. Forbrich, C. J. Lada, S. Meingast, Á. Hacar, J. Ascenso, C. Ackerl, B. Hasenberger, R. Köhler, K. Kubiak, I. Larreina, L. Linhardt, M. Lombardi, and T. Möller. VISION - Vienna survey in Orion. III. Young stellar objects in Orion A. *arXiv e-prints*, October 2018b.

Isabelle Joncour, Gaspard Duchêne, Estelle Moraux, and Frédérique Motte. Multiplicity and clustering in Taurus star forming region. II. From ultra-wide pairs to dense NESTs. *A&A*, 620:A27, November 2018. doi: 10.1051/0004-6361/201833042.

W. A. Joye and E. Mandel. *New Features of SAOImage DS9*, volume 295 of *Astronomical Society of the Pacific Conference Series*, page 489. 2003.

R. Köhler, M. G. Petr-Gotzens, M. J. McCaughrean, J. Bouvier, G. Duchêne, A. Quirrenbach, and H. Zinnecker. Binary stars in the Orion Nebula Cluster. *A&A*, 458:461–476, November 2006. doi: 10.1051/0004-6361:20054561.

Rainer Kohler and Christoph Leinert. Multiplicity of T Tauri stars in Taurus after ROSAT. *A&A*, 331:977–988, March 1998.

M. Kounkel, S. T. Megeath, C. A. Poteet, W. J. Fischer, and L. Hartmann. An HST Survey for 100-1000 au Companions around Young Stellar Objects in the Orion Molecular Clouds: Evidence for Environmentally Dependent Multiplicity. *ApJ*, 821: 52, April 2016. doi: 10.3847/0004-637X/821/1/52.

M. Kounkel, K. Covey, G. Suárez, C. Román-Zúñiga, J. Hernandez, K. Stassun, K. O. Jaehnig, E. D. Feigelson, K. Peña Ramírez, A. Roman-Lopes, N. Da Rio, G. S. Stringfellow, J. S. Kim, J. Borissova, J. G. Fernández-Trincado, A. Burgasser, D. A. García-Hernández, O. Zamora, K. Pan, and C. Nitschelm. The APOGEE-2 Survey of the Orion Star-forming Complex. II. Six-dimensional Structure. *AJ*, 156:84, September 2018. doi: 10.3847/1538-3881/aad1f1.

A. L. Kraus and L. A. Hillenbrand. The Coevality of Young Binary Systems. *ApJ*, 704: 531–547, October 2009. doi: 10.1088/0004-637X/704/1/531.

Adam L. Kraus, Michael J. Ireland, Frantz Martinache, and Lynne A. Hillenbrand. Mapping the Shores of the Brown Dwarf Desert. II. Multiple Star Formation in Taurus-Auriga. *ApJ*, 731(1):8, April 2011. doi: 10.1088/0004-637X/731/1/8.

Adam L. Kraus, Michael J. Ireland, Daniel Huber, Andrew W. Mann, and Trent J. Dupuy. The Impact of Stellar Multiplicity on Planetary Systems. I. The Ruinous Influence of Close Binary Companions. *AJ*, 152(1):8, July 2016. doi: 10.3847/0004-6256/152/1/8.

P. Kroupa, C. A. Tout, and G. Gilmore. The effects of unresolved binary stars on the determination of the stellar mass function. *MNRAS*, 251:293–302, Jul 1991. doi: 10.1093/mnras/251.2.293.

C. J. Lada. Star formation - From OB associations to protostars. In M. Peimbert and J. Jugaku, editors, *Star Forming Regions*, volume 115 of *IAU Symposium*, pages 1–17, 1987.

C. J. Lada and B. A. Wilking. The nature of the embedded population in the Rho Ophiuchi dark cloud - Mid-infrared observations. *ApJ*, 287:610–621, December 1984. doi: 10.1086/162719.

Richard B. Larson. Star formation in groups. *MNRAS*, 272(1):213–220, January 1995. doi: 10.1093/mnras/272.1.213.

Ch. Leinert, H. Zinnecker, N. Weitzel, J. Christou, S. T. Ridgway, R. Jameson, M. Haas, and R. Lenzen. A systematic search for young binaries in Taurus. *A&A*, 278:129–149, October 1993.

Timothy C. Licquia and Jeffrey A. Newman. Improved estimates of the milky way's stellar mass and star formation rate from hierarchical bayesian meta-analysis. *ApJ*, 806(1):96, Jun 2015. ISSN 1538-4357. doi: 10.1088/0004-637x/806/1/96. URL http://dx.doi.org/10.1088/0004-637X/806/1/96.

M. Lombardi, J. Alves, and C. J. Lada. 2MASS wide field extinction maps. IV. The Orion, Monoceros R2, Rosette, and Canis Major star forming regions. *A&A*, 535: A16, November 2011. doi: 10.1051/0004-6361/201116915.

Marco Lombardi, Hervé Bouy, João Alves, and Charles J. Lada. Herschel-Planck dust optical-depth and column-density maps. I. Method description and results for Orion. *A&A*, 566:A45, June 2014. doi: 10.1051/0004-6361/201323293.

S. T. Megeath, R. Gutermuth, J. Muzerolle, E. Kryukova, K. Flaherty, J. L. Hora, L. E. Allen, L. Hartmann, P. C. Myers, J. L. Pipher, J. Stauffer, E. T. Young, and G. G. Fazio. The Spitzer Space Telescope Survey of the Orion A and B Molecular Clouds. I. A Census of Dusty Young Stellar Objects and a Study of Their Mid-infrared Variability. *AJ*, 144:192, December 2012. doi: 10.1088/0004-6256/144/6/192.

S. T. Megeath, R. Gutermuth, J. Muzerolle, E. Kryukova, J. L. Hora, L. E. Allen, K. Flaherty, L. Hartmann, P. C. Myers, J. L. Pipher, J. Stauffer, E. T. Young, and G. G. Fazio. The Spitzer Space Telescope Survey of the Orion A and B Molecular Clouds. II. The Spatial Distribution and Demographics of Dusty Young Stellar Objects. *AJ*, 151:5, January 2016. doi: 10.3847/0004-6256/151/1/5.

S. Meingast, J. Alves, D. Mardones, P. S. Teixeira, M. Lombardi, J. Großschedl, J. Ascenso, H. Bouy, J. Forbrich, A. Goodman, A. Hacar, B. Hasenberger, J. Kainulainen, K. Kubiak, C. Lada, E. Lada, A. Moitinho, M. Petr-Gotzens, L. Rodrigues, and C. G. Román-Zúñiga. VISION - Vienna survey in Orion. I. VISTA Orion A Survey. *A&A*, 587:A153, March 2016. doi: 10.1051/0004-6361/201527160.

Stefan Meingast, João Alves, and Marco Lombardi. VISION - Vienna Survey in Orion. II. Infrared extinction in Orion A. *A&A*, 614:A65, June 2018. doi: 10.1051/0004-6361/201731396.

K. M. Menten, M. J. Reid, J. Forbrich, and A. Brunthaler. The distance to the Orion Nebula. *A&A*, 474:515–520, November 2007. doi: 10.1051/0004-6361:20078247.

M. G. Petr, V. Coudé du Foresto, S. V. W. Beckwith, A. Richichi, and M. J. McCaughrean. Binary Stars in the Orion Trapezium Cluster Core. *ApJ*, 500: 825–837, June 1998. doi: 10.1086/305751.

I. Pillitteri, S. J. Wolk, S. T. Megeath, L. Allen, J. Bally, M. Gagné, R. A. Gutermuth, L. Hartman, G. Micela, P. Myers, J. M. Oliveira, S. Sciortino, F. Walter, L. Rebull, and J. Stauffer. An X-Ray Survey of the Young Stellar Population of the Lynds 1641 and Iota Orionis Regions. *ApJ*, 768:99, May 2013. doi: 10.1088/0004-637X/768/2/99.

Deepak Raghavan, Harold A. McAlister, Todd J. Henry, David W. Latham, Geoffrey W. Marcy, Brian D. Mason, Douglas R. Gies, Russel J. White, and Theo A. ten Brummelaar. A Survey of Stellar Families: Multiplicity of Solar-type Stars. *ApJS*, 190(1):1–42, Sep 2010. doi: 10.1088/0067-0049/190/1/1.

B. Reipurth, C. J. Clarke, A. P. Boss, S. P. Goodwin, L. F. Rodríguez, K. G. Stassun, A. Tokovinin, and H. Zinnecker. Multiplicity in Early Stellar Evolution. In Henrik Beuther, Ralf S. Klessen, Cornelis P. Dullemond, and Thomas Henning, editors, *Protostars and Planets VI*, page 267, January 2014. doi: 10.2458/azu_uapress_9780816531240-ch012.

Jr. Spitzer, Lyman. The Dynamics of the Interstellar Medium. II. Radiation Pressure. *ApJ*, 94:232, September 1941. doi: 10.1086/144328.

W. Sutherland, J. Emerson, G. Dalton, E. Atad-Ettedgui, S. Beard, R. Bennett, N. Bezawada, A. Born, M. Caldwell, P. Clark, S. Craig, D. Henry, P. Jeffers, B. Little, A. McPherson, J. Murray, M. Stewart, B. Stobie, D. Terrett, K. Ward, M. Whalley, and G. Woodhouse. The Visible and Infrared Survey Telescope for Astronomy (VISTA): Design, technical overview, and performance. *A&A*, 575:A25, March 2015. doi: 10.1051/0004-6361/201424973.

M. B. Taylor. *TOPCAT & STIL: Starlink Table/VOTable Processing Software*, volume 347 of *Astronomical Society of the Pacific Conference Series*, page 29. 2005.

Fred L. Whipple. Concentrations of the Interstellar Medium. *ApJ*, 104:1, July 1946. doi: 10.1086/144829.

List of Figures

List of Tables

List of Abbreviations

CC	companion candidate.
CF	companion fraction.
IR	infrared.
ITC	initial target catalog of YSOs.
MCO	resulting multiplicity catalog for Orion A.
MF	multiplicity fraction.
MS	Main Sequence.
ONC	Orion Nebula Cluster.
PSF	point spread function.
SED	spectral energy distribution.
YSO	young stellar object.

Acknowledgements

Due to my busy life as a singly mother, the road of finishing this thesis was long. Therefore, the people that guided and accompanied me, and that deserve my honest gratitude, are numerous. This list can only mention a few of them, while it is not possible to put any order to it.

One of the most important people who lead to the success of this work is Monika Petr-Gotzens. During my stay at ESO she tried to share as much as possible of her endless knowledge with me, with incredible patience. I feel that I never learned more than during this time and I deeply enjoyed it. After my stay at ESO, Stefan Meingast took over the role of my co-supervisor. Most importantly, he provided one of the key datasets that I used in this work and taught me everything I needed to know about it. I am very certain, that Stefan must have been annoyed by the countless questions I asked him but he never let me feel that. Instead, he always helped me to see things clearer when I was stuck and always tried to cheered me up. He even visited me in the hospital once, when I was very sick. I will never forget that. Another important data provider is Josefa Großschedl. She taught me a lot about her YSO catalog and Orion A, patiently answered all of my questions, and helped me with editing and improving my applications to various conferences. Along with Stefan and Josefa, Verena Fürnkranz, Kieran Leschinski, Birgit Hasenberger, Sebastian Ratzenböck, Gabor Herbst-Kiss, and Irati Larreina Pinto always gave me helpful feedback and advice. Above that, they made the university feel like home. Two people whom I also want to thank, are Rainer Köhler and Karolina Kubiak. They put a lot of effort in helping me to correct some of my mistakes, understand my results, and apply for observing time at ESO. The link between all of these people is my supervisor, Joao Alves. He is the leader and the glue to our group. He (alongside with Monika) made my stay at ESO possible and encouraged and enabled me to attend multiple conferences where I had the chance to meet inspiring people from across the world. Joao himself is one of the most inspiring scientists I know. With his brilliant mind he always sees more than anybody else. His enthusiasm reignited the science fire in me multiple times. Joao, together with Monika and Charles Lada,

whom I had the chance to meet at two of the conferences, taught me an important lesson for life, which is, that truly successful people never loose respect of new or different ideas and the people who have them.

Another person who had an important impact on this thesis is Andrew Winter. He helped me to view my results from different angles and understand them better, due to the many fruitful discussions.

The road to this thesis did of course not begin with this project, but much before, when I took the decision to study Astronomy. After many years of working and being a mother I felt like an a bit of an outsider on my first days as a student. However, as I have always experienced among astronomers, my colleagues very quickly let me forget our different routes and made me feel like a part of their family. One of the most important members of this astronomer family is Markus Rockenbauer. It is impossible to count the many times when he left his own struggles behind to help me and others with his seemingly endless practical knowledge. I honestly think, that I would not have made it to the end of the road if it was not for Markus. Apart from that, he always makes me smile.

My interest in Astrophysics was triggered by my first and amazing physics teacher, Mag. Martin Glatz, and my beloved brother, Bernhard Ackerl, who seemingly always had an answer to my questions about how things work on Earth and in the Universe. While these two triggered my interests, it was due to my parents, Irmgard and Rudolf Ackerl, that I was able to make the dream of becoming an Astronomer true. Without their help, none of this would have been possible. As one of the first women in Austria who studied computing, my mum was also a great role model for me. She is one of the strongest women I know and made me believe that I can achieve everything, if I really want it.

I also owe my gratitude to Sigrid and Hannes Steinbauer, who made my stay at ESO possible, by making sure my son had all he needed while I was away, together with Carl Neumayr, who also helped me out with my statistics questions. Apart from them, I am deeply thankful for the support of Nicole Freißmuth, who always had an open door and ear, a warm meal, lots of love, and precious advice for me and my son.

Finally, I want to thank my son, Leon Ackerl, as he was the bravest, most patient person to accompany me on this road. It was certainly not easy to accept the numerous times where I had to study or work long days and nights, but he never stopped believing in me and always encouraged me to keep going, because in his opinion, my work was too important to stop. This is why I dedicate this work to him alongside with my mother.